Refining the Evolution of Gas-Particle Partitioning in Cooking Emissions Oxidation via FIGAERO-CIMS Analysis

Supplemental Information

Ruizhe Shen[1], Song Guo[1,2]*, Hui Wang[1], Ying Yu[1], Zichao Wan[1], Rui Tan[1], Wenfei Zhu[1], Zheng Chen[1], Shiyi Chen[1], Zhijun Wu[1], Shuangde Li[3], Yunfa Chen[3], Min Hu[1]

[1] *State Key Laboratory of Regional Environment and Sustainability, International Joint Laboratory for Regional Pollution Control, Ministry of Education (IJRC), College of Environmental Sciences and Engineering, Peking University, Beijing, 100871, China*

[2] *Collaborative Innovation Center of Atmospheric Environment and Equipment Technology, Nanjing University of Information Science & Technology, Nanjing 210044, China*

[3] *State Key Laboratory of Multiphase Complex Systems, Institute of Process Engineering, Chinese Academy of Sciences, Beijing 100190, China*

Corresponding author:

*Song Guo - State Key Laboratory of Regional Environment and Sustainability, International Joint Laboratory for Regional Pollution Control, Ministry of Education (IJRC), College of Environmental Sciences and Engineering, Peking University, Beijing, 100871, China; Email: songguo@pku.edu.cn

This PDF file includes:

Supplementary text S1-S6

Supplementary Tables S1-S20

Supplementary Figures S1-S56

S1. OH exposure estimation method in the Go:PAM flow tube

Experiments apply OFR254 mode of Go:PAM flow tube, where OH radical serve as the main oxidant. The OFR 254 mode generate OH radical from reaction of $O(^1D)$ radical and water vapor. $O(^1D)$ radicals are generated by photolysis of ozone[1].The reactions are listed in RS1-RS3:

$$O_3 \xrightarrow{hv\ 254nm} O(^1D) + O_2 \tag{RS1}$$

$$O(^1D) + H_2O \rightarrow 2OH \tag{RS2}$$

$$OH + precursors \rightarrow products \tag{RS3}$$

We estimate OH exposure in the flow tube using semi-empirical equation recommended by Peng et al[2] as shown in the main text. EqS1 represents the equation.

$$\log_{10} OH\ exposure(molecules\ cm^{-3}) = 15.514 + 0.79292 * \log_{10}[H_2O] + 0.023076 *$$
$$(\log_{10}[H_2O])^2 - 1.0238 * \log_{10}[\Phi_{254}] + 0.060786 * (\log_{10}[\Phi_{254}])^2 - \log_{10}\{exp[-0.42602 -$$
$$\log_{10}([O_3]/OHR)/0.39479]\} + \log_{10}(t_R/180) \tag{Eq. S1}$$

In equation S1, $[H_2O]$ stand for dimensionless water vapor mixing ratio in the flow tube that is converted from relative humidity data. Φ_{254} means total photon flux of the flow tube's ultraviolet lamp at 254nm. The Φ_{254} in the Go:PAM flow tube used in the experiments are determined by comparison between photometer measurement and ozone blank experiment estimation, quantified to be 6.05×10^{15} photons cm^{-2} s^{-1}. $[O_3]$ is ozone concentration in ppbv monitored by ozone analyzer. t_R is retention time of the OFR that is 55 second in current study. OHR is total OH reactivity in the flow tube. OHR is estimated based on VOCUS-PTR quantification of gas-phase organic compounds. For compounds with certain elemental composition detected by VOCUS, we search organic species in the National Cancer Institute (NCI) database to find molecules with same elemental composition, and summarize OH reaction rate constants provided by EPI SUITE™. We choose geometric mean of OH reaction rates provided by EPI SUITE™ as the rate coefficient corresponding to molecules with same elemental composition detected by VOCUS[3, 4]. Validation on applicability of equation S1 to our Go:PAM OFR is tested by sulfur dioxide-oxidation calibration experiment, using OH exposure result from SO_2 decay and a simple chemistry model[5] representing OH generation and decay in flow tubes. Reactions used in the chemistry model are shown in Table S1, while comparison

between OH exposures from equation S1, measured SO_2 decay and chemistry model are shown in Figure S1. Wall loss of primary aerosols is shown in Figure S2.
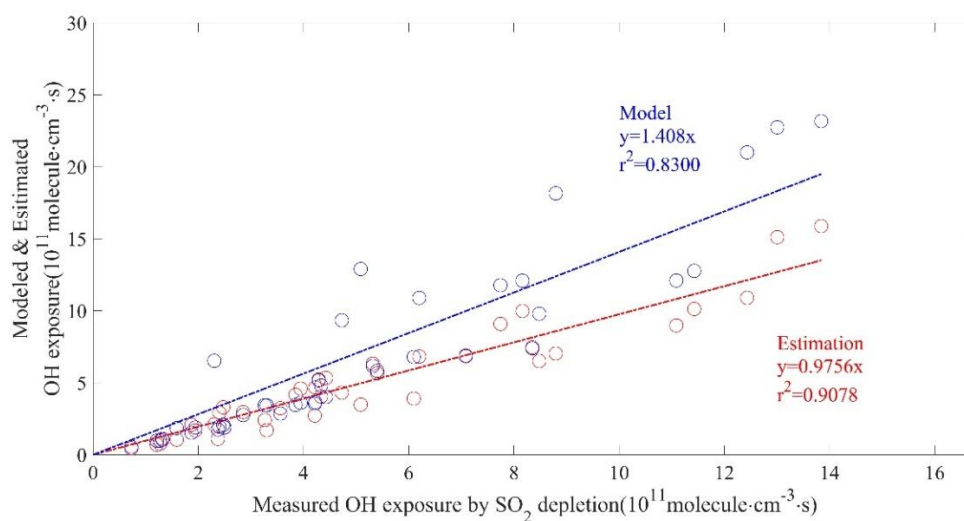
Figure S1 Correlation between OH exposure estimated by SO_2 depletion, chemistry model equation S1 in the Go:PAM reactor used in this experiment
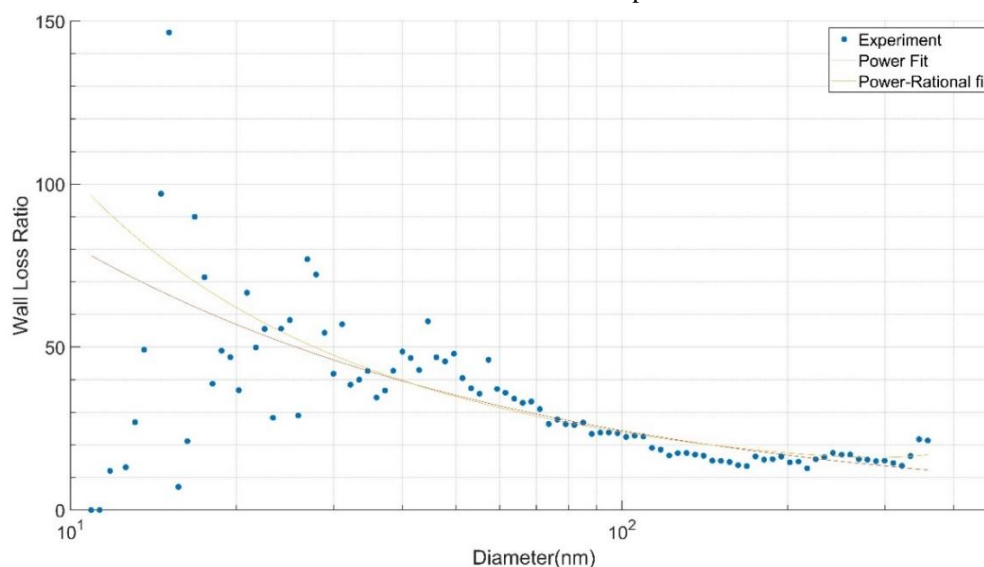
Figure S2 Size dependence of particle wall loss ratio in Go:PAM during experiment

Table S1 Reactions and rate constant used in box model calculation

Reaction	k(molecule·cm⁻³·s⁻¹) **
(1) $O_3 = O(^1D) + O_2(^1\Delta_g)$	$6.15\times10^{-2}(s^{-1})$ *
(2) $O_3 = O(^3P) + O_2$	$6.81\times10^{-3}(s^{-1})$ *
(3) $O(^3P) + O_2 = O_3$	1.39×10^{-14}
(4) $O(^3P) + O_3 = 2O_2$	8.0×10^{-15}
(5) $O(^1D) + N_2 = O(^3P) + N_2$	2.6×10^{-11}
(6) $O(^1D) + O_2 = O(^3P) + 0.15O_2 + 0.05O_2(^1\Delta_g) + 0.8O2(^1\Sigma_g)$	4.0×10^{-12}
(7) $O(^1D) + O_3 = 1.5O_2 + O(^3P)$	2.4×10^{-10}

(8) $O_2(^1\Delta_g) + O_2 = 2O_2$ 1.6×10^{-18}

(9) $O_2(^1\Delta_g) + O_3 = 2O_2 + O(^3P)$ 3.8×10^{-15}

(10) $O_2(^1\Delta_g) + H_2O = O_2 + H_2O$ 5.0×10^{-18}

(11) $O_2(^1\Delta_g) + O_2(^1\Delta_g) = 1.1O_2 + 0.9O_2(^1\Sigma_g)$ 2.8×10^{-17}

(12) $O_2(^1\Sigma_g) + N_2 = 0.1O_2 + 0.9O_2(^1\Delta_g) + N_2$ 2.1×10^{-15}

(13) $O_2(^1\Sigma_g) + H_2O = 0.1O_2 + 0.9O_2(^1\Delta_g) + N_2$ 4.6×10^{-12}

(14) $O_2(^1\Sigma_g) + O_3 = 1.43O_2 + 0.3O_3 + 0.27O_2(^1\Delta_g) + 0.7*O(^3P)$ 2.2×10^{-11}

(15) $O(^1D) + H_2O = 2OH$ 2.2×10^{-10}

(16) $O(^3P) + OH = H + O_2$ 3.5×10^{-11}

(17) $H + O_2 = HO_2$ 1.19×10^{-12}

(18) $HO_2 + O(^3P) = OH + O_2$ 5.8×10^{-11}

(19) $HO_2 + OH = H_2O + O_2$ 1.1×10^{-10}

(20) $H + O_3 = OH + O_2$ 2.9×10^{-11}

(21) $H + HO_2 = 1.8OH + 0.07H_2 + 0.07O_2 + 0.03H_2O + 0.03O(^3P)$ 8.0×10^{-11}

(22) $H + OH = H_2O$ 1.89×10^{-11}

(23) $OH + OH = H_2O_2$ 5.2×10^{-12}

(24) $OH + OH = H_2O + O(^3P)$ 1.5×10^{-12}

(25) $OH + H_2O_2 = H_2O + HO_2$ 1.7×10^{-12}

(26) $OH + O_3 = HO_2 + O_2$ 7.3×10^{-14}

(27) $HO_2 + HO_2 = H_2O_2 + O_2$ 2.9×10^{-12}

(28) $HO_2 + O_3 = OH + 2O_2$ 2.0×10^{-15}

(29) $H_2O_2 + O(^3P) = OH + HO_2$ 1.7×10^{-15}

(30) $H_2O_2 = 2OH$ $4.78\times10^{-4}(s^{-1})$ *

(31) $OH + SO_2 = HSO_3$ 8.04×10^{-13}

(32) $HSO_3 + O_2 = SO_3 + HO_2$ 4.30×10^{-13}

(33) $O(^3P) + SO_2 = SO_3$ 3.10×10^{-14}

(34) $SO_3 + H_2O = H_2SO_4$ 3.14×10^{-15}

(35) $O(^1D) + H_2 = OH + H$ 1.1×10^{-10}

---

*Estimated from UV spectra data in the Go:PAM

**Rate constant data source[6]

S2. VOCUS & FIGAERO sensitivity/volatility calibration

For VOCUS data quantification, we utilize authentication standard gas mixture to calibrate the response of 25 VOCs in VOCUS with different composition and structure. Calibrations were

performed every day after the experiments finished at standard concentration 1, 10, 20 50, and 100ppbv. The standard gas includes 7 aromatic hydrocarbons (benzene, toluene, m-xylene, styrene, 1,2,3-trimethylbenzene, 1,3,5-trimethylbenzene, naphthalene), 5 terpenes and terpenoids (isoprene, α-pinene, β-pinene, β-caryophyllene, nopinone), 5 carbonyl compounds (acetaldehyde, acrolein, acetone, methyl vinyl ketone, 3-pentanone, ethyl acetate), 3 alcohols (methanol, 2-propanol, 1-butanol), 2 nitriles (acrylonitrile, acetonitrile), and 2 halocarbons (chlorobenzene, 1,3-dichlorobenzene). For species detected with same elemental composition with any species among the standard gas, we choose the sensitivity of the compound in the standard standing for their sensitivity. For species detected having different elemental composition other than species in the standard gas, we divide species into elemental categories by having certain elemental abundant in the molecule (e.g. CH compounds, CHO compounds, CHON compounds) for convenience. We select the geometry mean sensitivity among compounds with same elemental category in the standard gas to represent the sensitivity of compounds in the whole group. The sensitivity data are used for OH exposure calculation[7].

Quantification and volatility determination using FIGAERO-CIMS are completed utilizing calibration methods employed by Ylisirniö[8]. Schematic view of calibration process is shown in Fig S2 a). During sensitivity calibration, sensitivity of certain compound is determined by depositing certain volume of authentication standard solution onto PTFE filter inside FIGAERO inlet, and process one operation cycle with thermal desorption phase only. We choose acetonitrile as the solvent for better solvation and wetting ability on the filter. In the experiment, we deposit 3-5 different volume within the volume range 1μL -20μL of standard solution with concentration ~1μg/mL onto the filter, proceed the thermal desorption cycle, and count the target compound-iodide ion during the desorption process. Sensitivity of selected compound in CIMS is determined by equation S2:

$$\overline{([RI^-]/[I^-])} = S_i(ncps \cdot ppb^{-1}) \times V \times c \times \frac{RT}{pQ_{TD}\Delta t_{TD}} + \overline{([RI^-]/[I^-])}_{blank} \quad (\text{Eq. S2})$$

In Equation S2, [RI-]/[I-] stands for average normalized signal of selected compound during the thermal desorption process whose normalization based on reagent ion (iodide ion) signal, ([RI-]/[I-])blank for normalized signal during blank samples, V for total volume of standard solution deposited in μL, c for standard solution concentration in μg/mL, T for room temperature in Kelvin,

p for atmospheric pressure in Pa, Q_{TD} for carrier gas flow rate during thermal desorption in m^3/min, Δt_{TD} for thermal desorption duration in minutes. In calibration of this study, Q_{TD} is 0.002 m^3/min, and Δt_{TD} is 45min, longer than 35min in experiment setup. The final sensitivities are given by linear regression between normalized signal [RI-]/[I-] and solution deposition volume V. For volatile compounds such as formic acid and acetic acid, calibration is completed by generating standard gas from penetration tube, then process linear fit between normalized ion counts and standard gas concentration.

For signals without corresponding standard compound and thus lack direct sensitivity calibration, we use 2-D VBS proxy to determine the sensitivity. Briefly, we put compounds detected by CIMS into 2-D VBS space using parameterization shown in Section S3. Then, we proceed k-means clustering algorithm built in MATLAB® on compounds in the 2-D VBS space, divide these compounds into several groups as shown in Fig. S3. Next, we distribute standard compounds with known sensitivity into 2-D VBS space, finding out each group's corresponding standard compound adapting KNN classification model from clustering results. Finally, we set the sensitivity of compounds having molecular formula different from all of the calibrated compounds to geometry mean sensitivity of standard compounds in the same group. These results could help improve characterization and quantification of species detected by CIMS by species and in 2-D VBS framework.

Volatility determination by FIGAERO is based on log-linear correlation between desorption temperature while signal reaches its peak[9]. Volatility calibrations is proceeded choosing polyethylene glycol (PEGs) as standard compound. Calibrations are proceeded following experiment setup in Fig. S2 b). Standard solution of PEGs is generated by dissolve PEG standard in acetonitrile, then atomized and deposited onto the filter. For other standard solution, we used same method as sensitivity calibration to achieve relation between desorption peak temperature. The result empirical log-linear relation between peak temperature T_{max} at room temperature and saturation vapor pressure p_0 from PEGs are shown in Equation S3.

$$\log_{10} p_{0,298K} = 21.9 - 0.072 T_{max}(K) \; R^2 = 0.94 \qquad \text{(Eq. S3)}$$
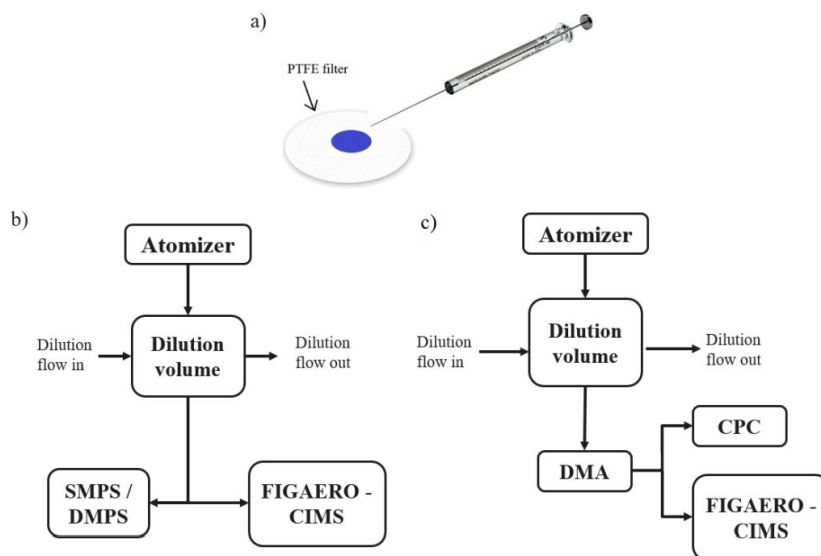
Figure S3 FIGAERO-CIMS volatility and sensitivity calibration method introduced by Ylisirniö, A., et al. (2021) that is used in this article. a) Illustration of the syringe deposition method. b) & c) Illustration of the polydisperse & monodisperse deposition method

Table S2 Sensitivity of calibrates used in CIMS sensitivity calibration and 1σ confidence interval

Species	Molecular composition	Sensitivity (ncps ppb^{-1}) **
PEG-7	$C_{14}H_{30}O_8$	$9.3_{9.0}^{11.2} \times 10^{-2}$
PEG-8	$C_{16}H_{34}O_9$	$10.8_{4.43}^{18.4} \times 10^{-3}$
Malonic acid	$C_3H_4O_4$	Decomposition
Succinic acid	$C_4H_6O_4$	$7.6_{5.8}^{9.5} \times 10^{-3}$
Glutaric acid	$C_5H_8O_4$	$7.3_{4.8}^{10.3} \times 10^{-3}$
Adipic acid	$C_6H_{10}O_4$	$8.2_{5.3}^{11.6} \times 10^{-3}$
Pimelic acid	$C_7H_{12}O_4$	$8.7_{6.2}^{11.5} \times 10^{-3}$
Suberic acid	$C_8H_{14}O_4$	$1.7_{1.5}^{1.9} \times 10^{-2}$
Azelaic acid	$C_9H_{16}O_4$	$7.7_{4.8}^{11.1} \times 10^{-3}$
Sebacic acid	$C_{10}H_{18}O_4$	$7.4_{5.5}^{9.4} \times 10^{-3}$
Dodecanedioic acid	$C_{12}H_{22}O_4$	$3.6_{2.3}^{5.1} \times 10^{-3}$
D-Camphoric acid	$C_{10}H_{16}O_4$	$7.8_{0.84}^{8.5} \times 10^{-3}$
Pinonic acid	$C_{10}H_{16}O_3$	$1.1_{0.66}^{1.7} \times 10^{-2}$
Citric acid	$C_6H_8O_7$	not detected
1,2,4-Tricarboxylic acid	$C_7H_{10}O_6$	not detected
1,3,5-Pentanetricarboxylic acid	$C_8H_{12}O_6$	not detected
2-Hydroxy-1-cyclohexanone	$C_6H_{10}O_2$	not detected
Hydroxyacetone	$C_3H_6O_2$	not detected
DL-Lactic acid	$C_3H_6O_3$	$4.6_{2.3}^{7.6} \times 10^{-2}$
DL-Glyceric acid	$C_3H_6O_4$	$6.3_{0.0}^{32} \times 10^{-4}$
Erythritol	$C_4H_{10}O_4$	$1.2_{1.0}^{1.5} \times 10^{-2}$
2-D-Deoxyribose	$C_5H_{10}O_4$	$1.5_{1.1}^{1.9} \times 10^{-2}$
Xylitol	$C_5H_{12}O_5$	$1.1_{0.96}^{1.3} \times 10^{-2}$

Levoglucosan	$C_6H_{10}O_5$	$3.8^{5.2}_{2.5} \times 10^{-2}$
Isosorbide mononitrate	$C_6H_9NO_6$	$3.5^{5.6}_{1.7} \times 10^{-2}$
2-Nitrophenol	$C_6H_5NO_3$	$1.2^{2.6}_{0} \times 10^{-4}$
4-Nitrophenol	$C_6H_5NO_3$	$1.6^{1.9}_{1.4} \times 10^{-1}$
4-Nitrocatechol	$C_6H_5NO_4$	$7.7^{9.2}_{6.5} \times 10^{-3}$
Benzoic acid	$C_7H_6O_2$	not detected
Salicylic acid	$C_7H_6O_3$	$1.9^{2.6}_{1.3} \times 10^{-3}$
Formic acid*	CH_2O_2	$7.5^{17.0}_{4.4} \times 10^{-3}$
Acetic acid*	$C_2H_4O_2$	$4.4^{17.0}_{2.4} \times 10^{-4}$

* Standard gas calibration generated by standard penetration tube

** Main text stands for sensitivity, superscript and subscripts stands for upper and lower bound of 1σ confidence interval
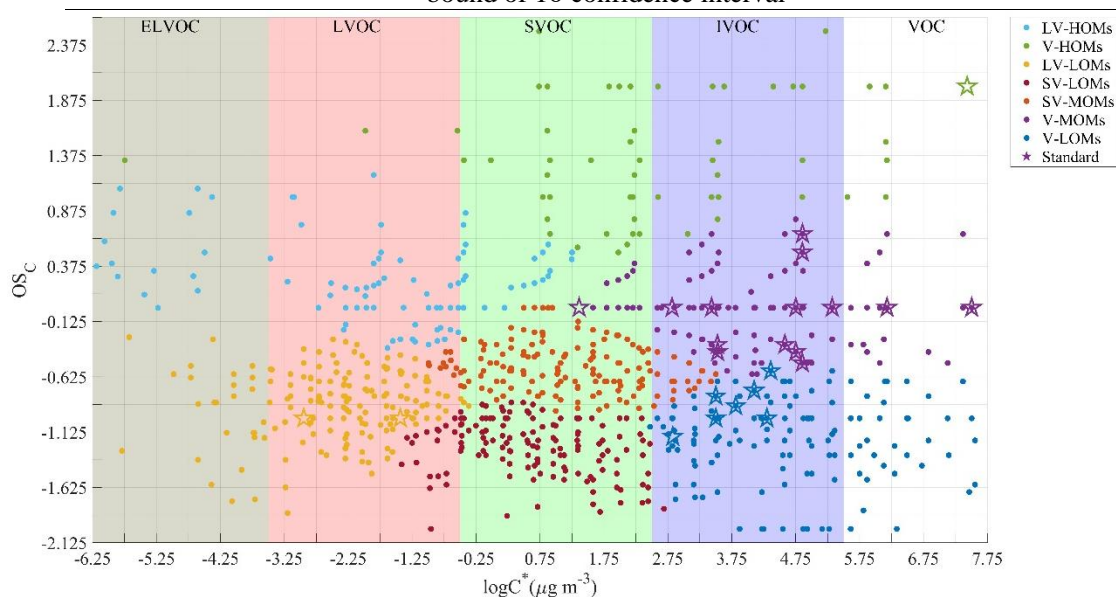
Figure S4 Distribution of species detected in cooking experiment by CIMS (colored dots) and standard compound with known sensitivity(stars)
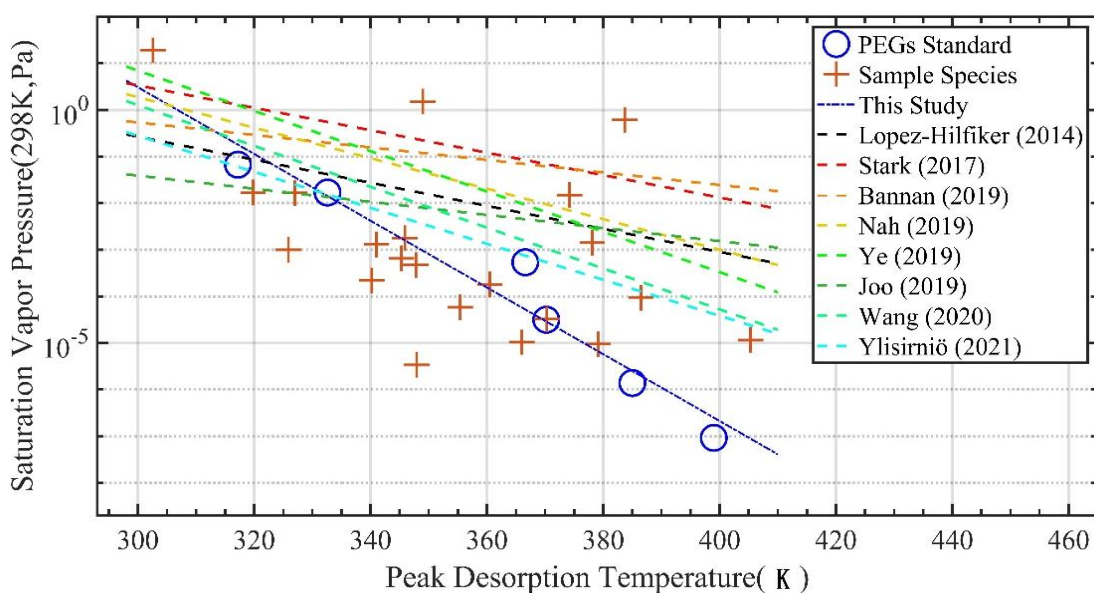
Figure S5 Correlation between FIGAERO thermal desorption peak temperature and satuartion vapor pressure of PEGs and OOMs in previous and current studies[8-15]

S3. 2-D VBS spacing

2-D VBS framework is firstly developed by Donahue in 2011[16]. The framework added Distribution of gas-phase and aerosol-phase organic compounds in 2-D VBS space are determined from molecular elemental composition detected by ToF-CIMS measurements. Parameterization used in this article is according to Li et al., as shown in Equation S4[17]:

$$\log_{10} C_0 = (n_C^0 - n_C)b_C - n_O b_O - 2\frac{n_C n_O}{n_C + n_O} b_{CO} - n_N b_N - n_S b_S \qquad \text{(Eq. S4)}$$

In Eq. S4, targeted saturation vapor concentration C_0 is determined by elemental composition and semi-empirical parameters. n_C, n_O, n_N, n_S are number of most abundant elements atmospheric in organic aerosols, n_C^0 stand for reference carbon number, b_C means influeance of molecular size on volatility, b_O, b_N, b_S shows effect of functional group containing O, N, and S atom, b_{CO} means polar- nonpolar interaction influence on volatility. Parameters used for compounds with different molecular composition given by Li et al. are shown in Table S3.

Table S3 Elemental composition class and corresponding parameters in Eq. S4

Elemental Composition Class	n_C^0	b_C	b_O	b_{CO}	b_N	b_S
CH	23.8	0.4861	--	--	--	--
CHO	22.66	0.4481	1.656	−0.7790	--	--
CHN	24.59	0.4066	--	-	0.9619	--
CHON	24.13	0.3667	0.7732	−0.07790	1.114	--
CHOS	24.06	0.3637	1.327	−0.3988	0	0.7579
CHONS	28.5	0.3848	1.011	0.2921	1.053	1.316

S4. Non-targeted analysis utilizing matrix factorization analysis

For complex mass spectrometry data, non-targeted analysis is introduced to achieve

characteristics quantities of detected species without reliable direct prior compound and structure information. Basic concept and data-process path are shown in Figure S6[18]. Matrix Factorization approaches has been introduced as crucial methods in non-targeted analysis. Briefly, Matrix Factorization is a dimension reduction approach that approximately divide a target m×n data matrix $\mathbf{X}$ containing hundreds of variables(n) and change through hundreds of time points(m) into p(unknown) different constant sources that varies with time, as shown in Equation S5. The source composition profile are shown in a n×p matrix $\mathbf{F}$, while the time series of the source are in the m× p matrix $\mathbf{G}$. Factorization target is to cover the difference between data matrix $\mathbf{X}$ and fitted matrix $\mathbf{R}$, minimizing the error matrix $\mathbf{E}$ toward the measurement uncertainty matrix $\boldsymbol{\sigma}$ of input data.

$$\mathbf{X} = \mathbf{GF} + \mathbf{E} = \mathbf{R} + \mathbf{E} \qquad\qquad \text{Eq. S5}$$

For a better factorization result, we compared two widely used factorization approaches for high-resolution mass spectrometry factor analysis processes: Multilinear Engine-2 Positive Matrix Factorization (ME-2 PMF) and Non-Negative Matrix Factorization (NNMF)[19]. ME-2 PMF is proceeded by utilizing Igor Pro® program SoFi® developed by Canonaco et al. [20]. NNMF is proceeded by built-in algorithm in MATLAB® [21]. To achieve better deconvolution result, and to avoid possible background signal interference or physical unreasonable factorization results, we also proceed three different data pre-treatment methods on input matrixes. These includes direct factorization of full time series data without further selection and pre-treatment other than basic data pre-treat methods developed by Buchholz et al. [22], normalize time series data to maximum for trend analysis, and particle-phase only data for volatility & oxidative state analysis. The Goodness of PMF and NNMF results are evaluated by global and local evaluation parameters. Global evaluation parameters include Q/Q_{exp}, root mean square error (RMSE), explained absolute variance $Ratio_{var}$, focusing on performance on the whole data set. Local parameters include time series of summed absolute relative residual and unexplained variation (UEV) among all ions[20, 22]. These parameters are defined below:

$$Q = \sum_{j=1}^{m} \sum_{i=1}^{n} \left(\frac{E_{ij}}{\sigma_{ij}} \right)^2 \qquad Q_{exp} = n \times m - p \times (p + m) \qquad\qquad \text{Eq. S6}$$

$$RMSE = \sqrt{\frac{\sum_{j=1}^{m} \sum_{i=1}^{n} (E_{ij})^2}{n \times m}} \qquad\qquad \text{Eq. S7}$$

$$Ratio_{var} = \frac{\sum_{ij}|R_{ij} - \overline{X_i}|}{\sum_{ij}|R_{ij} - \overline{X_i}|} \qquad \text{Eq. S8}$$

$$\text{Sum relative residual}_i = \frac{\sum_j R_{ij} - X_{ij}}{\sum_j |X_{ij}|} \qquad \text{Eq. S9}$$

$$\text{absolute relative residual}_i = \frac{\sum_j |R_{ij} - X_{ij}|}{\sum_j |X_{ij}|} \qquad \text{Eq. S10}$$

$$\text{UEV}_i = \frac{\sum_j |e_{ij}/\sigma_{ij}|}{\sum_j |X_{ij}/\sigma_{ij}|} \qquad \text{Eq. S11}$$

To obtain a reasonable result, UEV are expected to be less than 25%. Q/Q_{exp} are targeted to reduce to near 1. For best factor number, we firstly plot the relation between factor number and global goodness parameters, choose the "turning points" where goodness parameters decrease significantly slower after the point than before, which means the factor number is most efficient. Then, we examine the time series of local goodness parameters at and just after "turning points" to investigate if adding factor number at the turning point leading to significant developments of factorization result. Next, we look at thermogram during thermal desorption in FIGAERO operation, and finally choose reasonable factorization results. Global and local parameters are also used for determination of PMF&NNMF performance on proceeding factorization and thus choosing suitable factorization method and data pre-treat methods for CIMS data processes. Spectra contrast angle θ are used to assign the similarity of factors, treating spectra of each factor as vectors in linear space make up by species concentration[22, 23]. Determination of contrast angle are shown in Equation S12:

$$cos\theta = \frac{\sum_i a_i b_i}{\sqrt{\sum_i a_i^2 \sum_i b_i^2}} \qquad \text{Eq. S12}$$

In Equation S12, a_i and b_i stands for spectra intensity of different factors in MPF results. Two factors would be considered not similar if $\theta > 30°$[24]. Thus, a good PMF result should output factors with contrast angle $\theta > 30°$ between every two factors[22].

Figures S7-S9 show change of the global goodness parameters of ME-2 PMF and MATLAB® NNMF while adding factor number. MATLAB® NNMF performed better regarding global goodness parameters not considering measurement uncertainty such as lower RMSE and higher $Ratio_{var}$ especially at factor numbers below 10. However, while considering relationship between measurement uncertainty and factorization result bias using the Q/Q_{exp} parameter, ME-2 PMF

shows better performance. ME-2 PMF aim at minimize firstly the uncertainty of signal with lower measurement uncertainty, so the absolute relative residual time series of ME-2 PMF shows better performance than MATLAB® NNMF at relevant factor number of both factorization methods, as Figures S10-S12 depicted. The two methods have comparable bias only when data pre-treat method are selected to be normalizing the time series of detected ions to its maximum value, which mainly aiming at extracting changing patterns, and thus expect to resolve volatility of detected species. Among data processes, while utilizing ME-2 PMF as the factorization algorithm, as Figures S13-S15 show, full time-series data shows slightly better performance than particle-phase only data and obvious advantage over time series normalized to maximum point of each detected compound. On the contrary, MATLAB® NNMF method favors data process adopting normalized full time series than particle-phase only and full time series, especially at duration corresponding to measurement of primary cooking emissions, shown in Figures S16-S18. In conclusion, we would prefer choosing ME-2 PMF as factorization algorithm, select full time series data as main data pre-treat method factorization in this article, while compare results of particle-phase only data to volatility and partitioning results as reference. Table S5 shows contrast angle θ between factors of ME-2 PMF best results. The contrast angles are between every two factors are larger than 30° (minimum 35°), showing reasonable results of ME-2 PMF.

The factors obtained from PMF are classified with oxidative state and volatility. First, the 13th factor is considered contaminant factor, named Factor Unknown. The contamination factor consists of 3 separated peaks at totally separate desorption temperatures, implying that it may consist of three parts related to different interference. First part at low desorption temperature may contain interference from FIGAERO inlet model shifting that may mix gas-phase components with aerosol-phase, which can be observed at the first couple of seconds of particle phase data. Next two parts at higher desorption temperature may come from residuals of semi-volatile and low-volatile residuals. 12 interpretable factors are classified as 3 categories, considering its volatility represented by FIGAERO-CIMS measured gas-particle partitioning coefficient K_p. Factors mainly or even almost present in gas phase are named volatile factors "Vx", factors abundant in both gas phase and aerosol phase factors are called semi-volatile factors "SVx", and mostly particle phase factors are classified low-volatile factors "LVx". Factors among each volatility categories are further distinguished and numbered by its oxidative state. Lower number

in factor name such as Factor V1 and SV1 are related to primary components, while reaching

higher abundance at low oxidative states. Medium number factors, namely Factor V2LV1 and

SV2, correspond to intermediate oxidative states, consist of first-generation products. Factors with

number ≥3 in their name represent highly oxidated products that relate to multi-generation

oxidation.
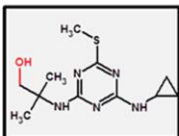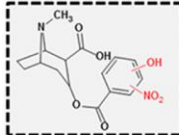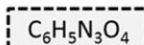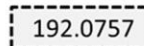
Figure S6 Brief concept of non-targeted analysis in high-resolution mass spectrometry
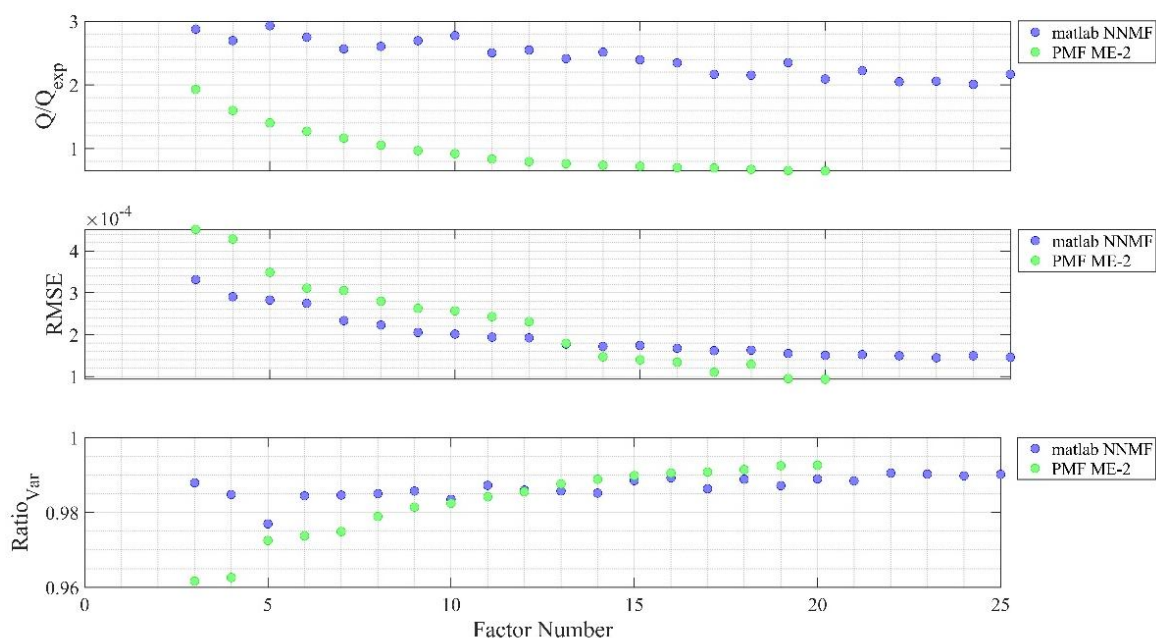
Figure S7 Evolution of global goodness parameters Q/Q_{exp}, RMSE, and $Ratio_{Var}$ while adding factor number to ME-2 PMF & MATLAB® NNMF results using full FIGAERO-CIMS data time series as factorization input.
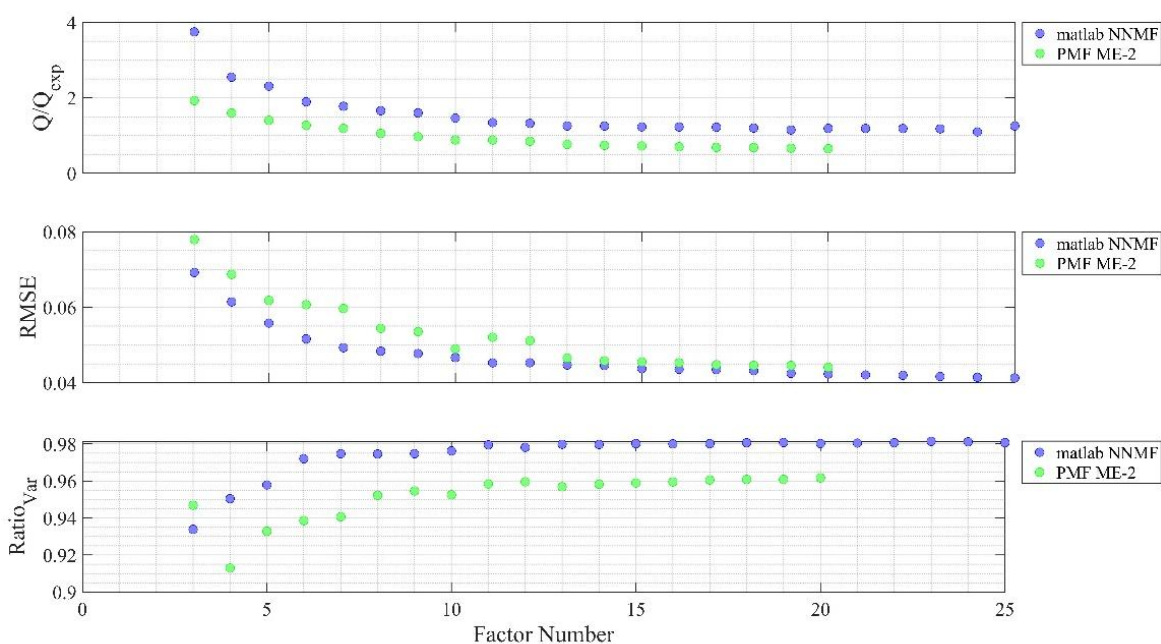
Figure S8 Evolution of global goodness parameters Q/Q_{exp}, RMSE, and $Ratio_{Var}$ while adding factor number to ME-2 PMF & MATLAB® NNMF results using normalized FIGAERO-CIMS data time series as factorization input
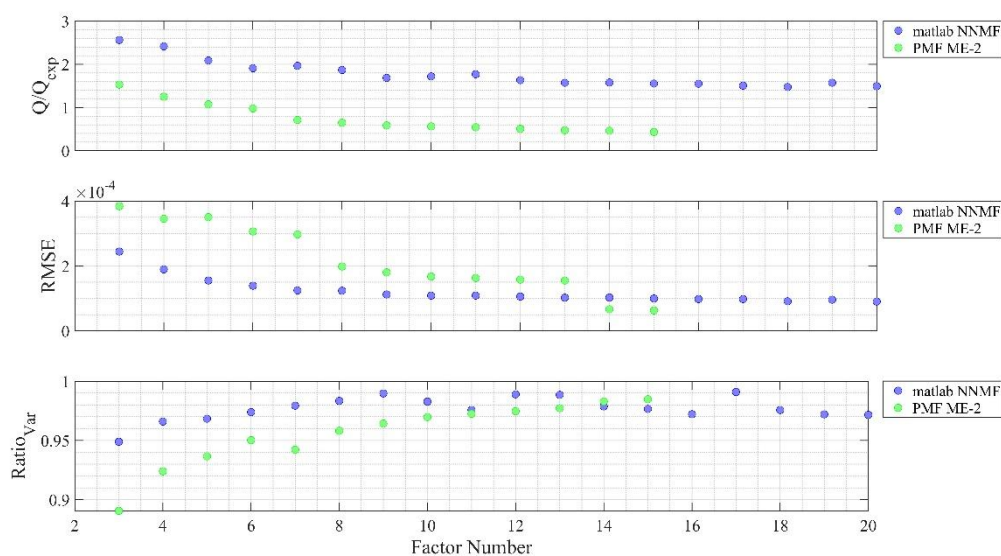
Figure S9 Evolution of global goodness parameters Q/Q_{exp}, RMSE, and $Ratio_{Var}$ while adding factor number to ME-2 PMF & MATLAB® NNMF results using particle-phase only FIGAERO-CIMS data time series as factorization input

Table S4 Possible best factor number list of factorization algorithms with various data pre-treat methods. Bold number shows the best factor number among results in certain factorization and pre-treat method

Possible best factor number	Full time series	Normalized full time series	Particle-phase only
ME-2 PMF	6,10,11,**13**,15	8,11,**13**,15	**8**,9,12,14
MATLAB® NNMF	6,**10**,15	7,**11**,15	**6**,9,12
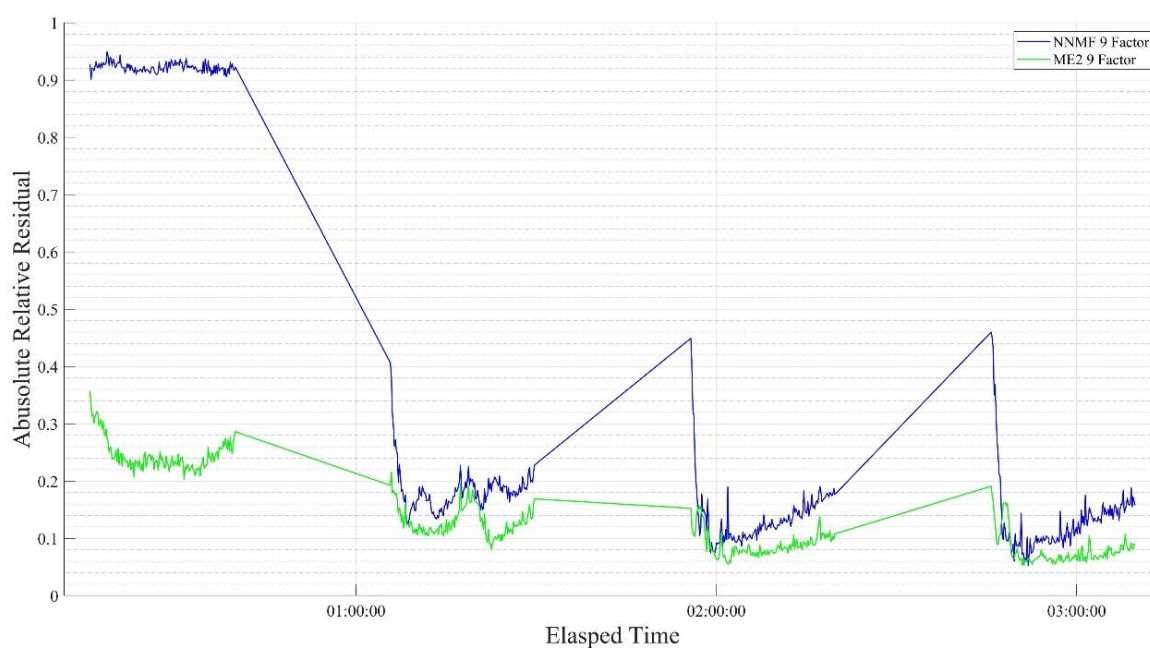
Figure S10 Time series of absolute relative residual for MATLAB® NNMF results (blue line) and ME2 results (green line) of particle-phase only FIGAERO-CIMS datasets at selected 'best' factor numbers
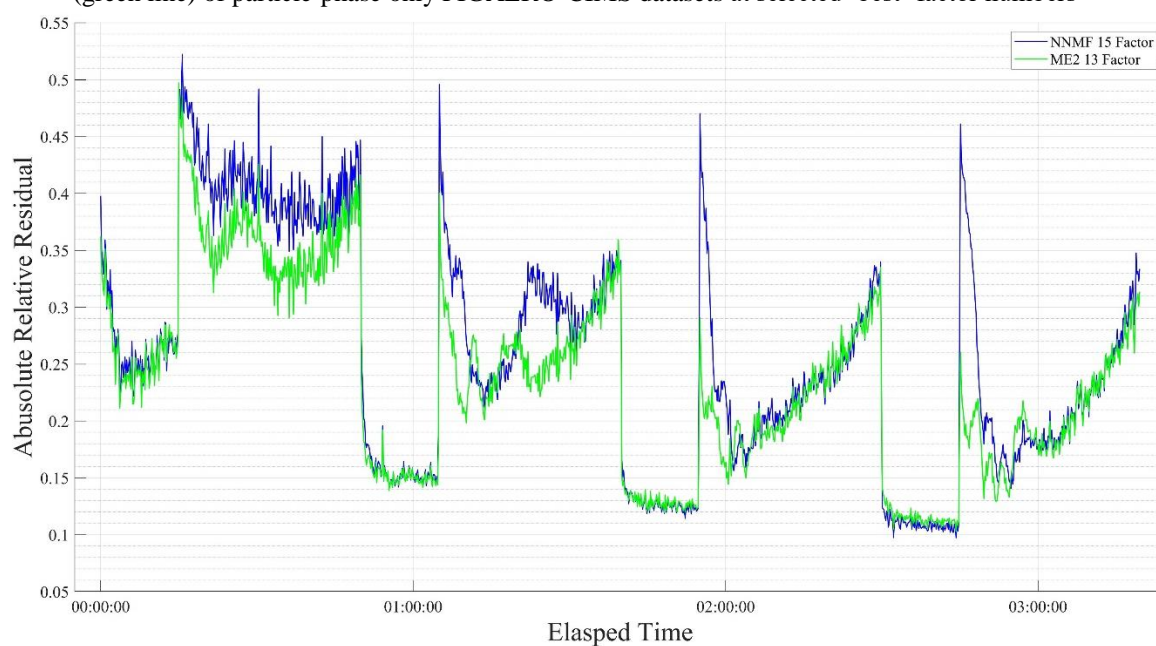
Figure S11 Time series of absolute relative residual for MATLAB® NNMF results (blue line) and ME2 results (green line) of FIGAERO-CIMS datasets normalized to maximum value in the time series at selected 'best' factor numbers
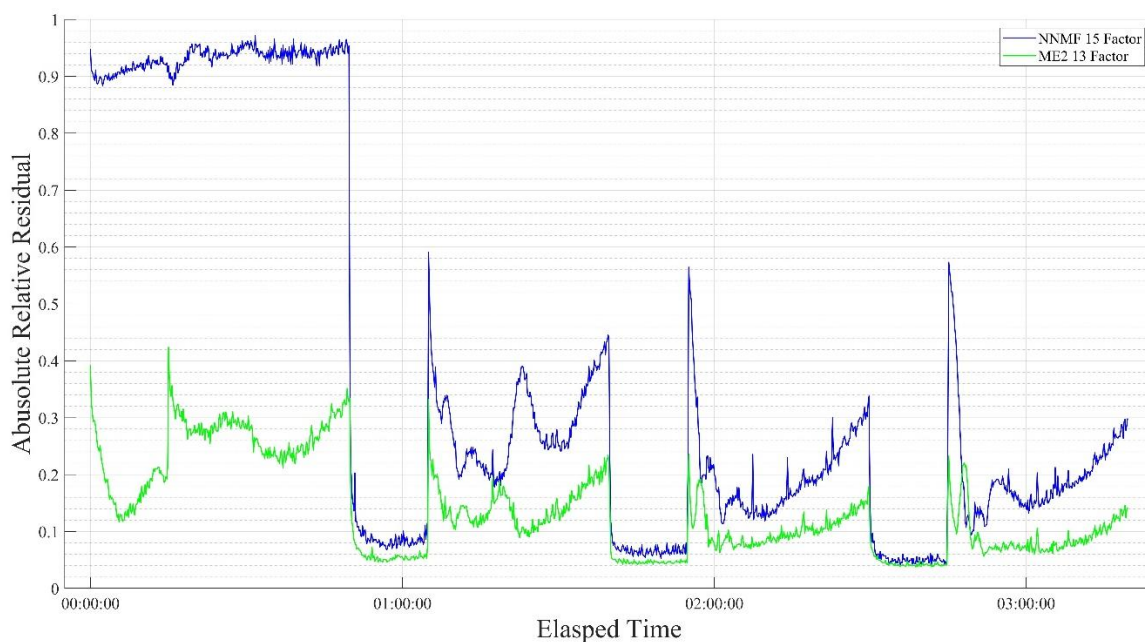
Figure S12 Time series of absolute relative residual for MATLAB® NNMF results (blue line) and ME2 results (green line) of FIGAERO-CIMS normal datasets at selected 'best' factor numbers
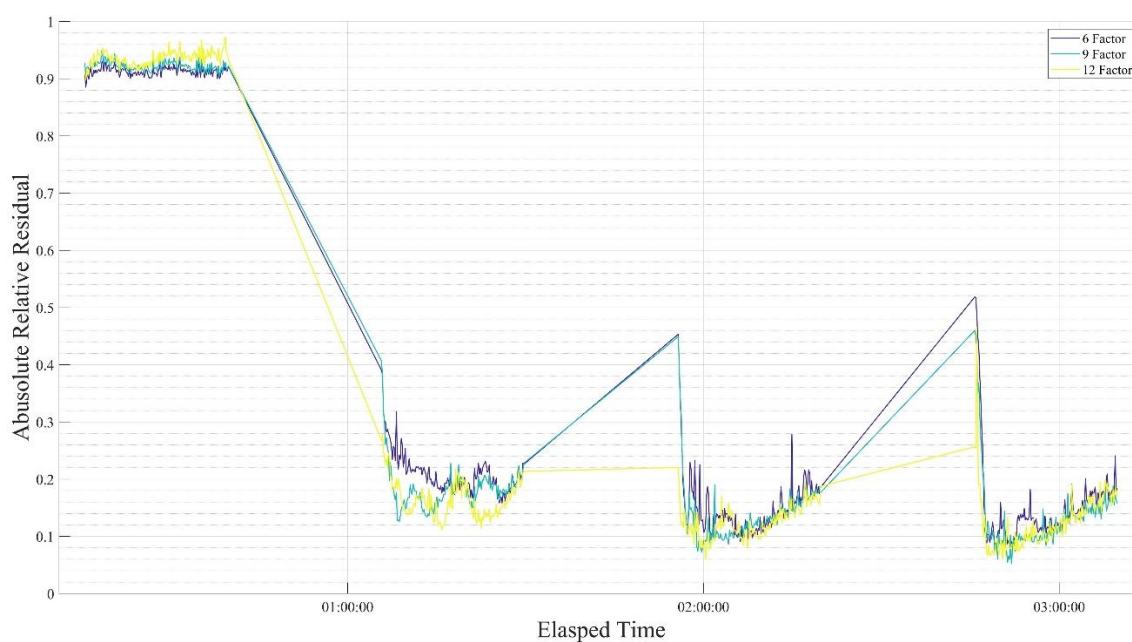
Figure S13 Detailed absolute relative residual time series of factorization results of particle-phase only data utilizing MATLAB NNMF at factor number 6, 9 and 12 which are selected to be right at "turning points"
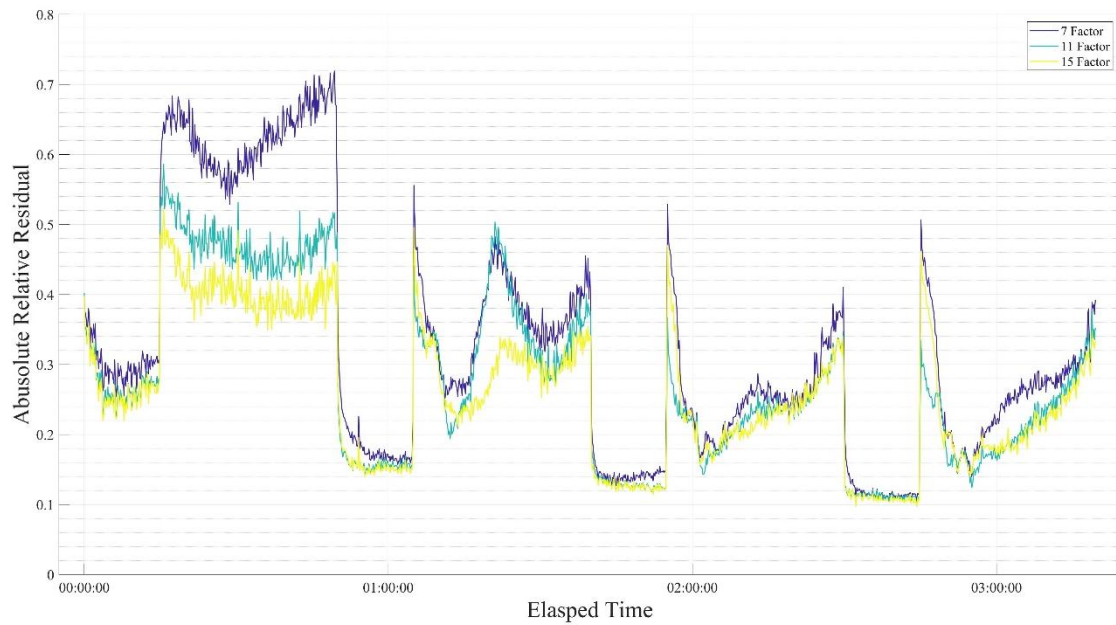
Figure S14 Detailed absolute relative residual time series of factorization results of normalized full time-series data utilizing MATLAB NNMF at factor number 7,11 and 15 which are selected to be right at "turning points"
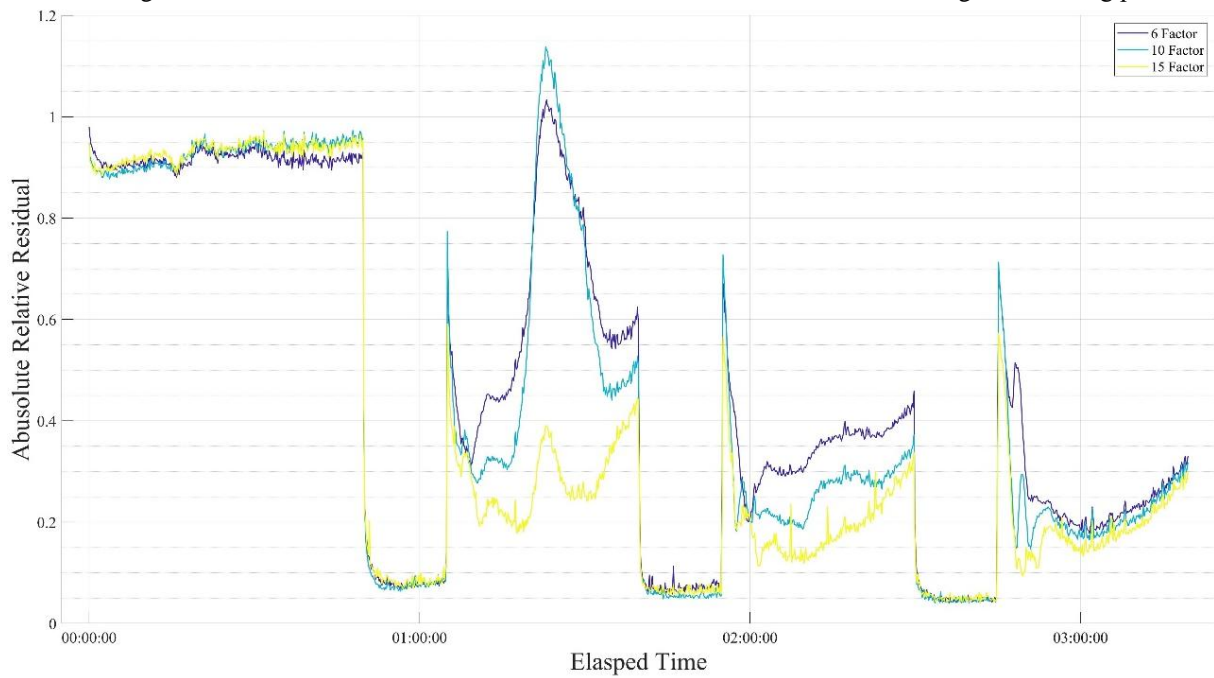
Figure S15 Detailed absolute relative residual time series of factorization results of full time-series data utilizing MATLAB NNMF at factor number 6,10 and 15 which are selected to be right at "turning points"
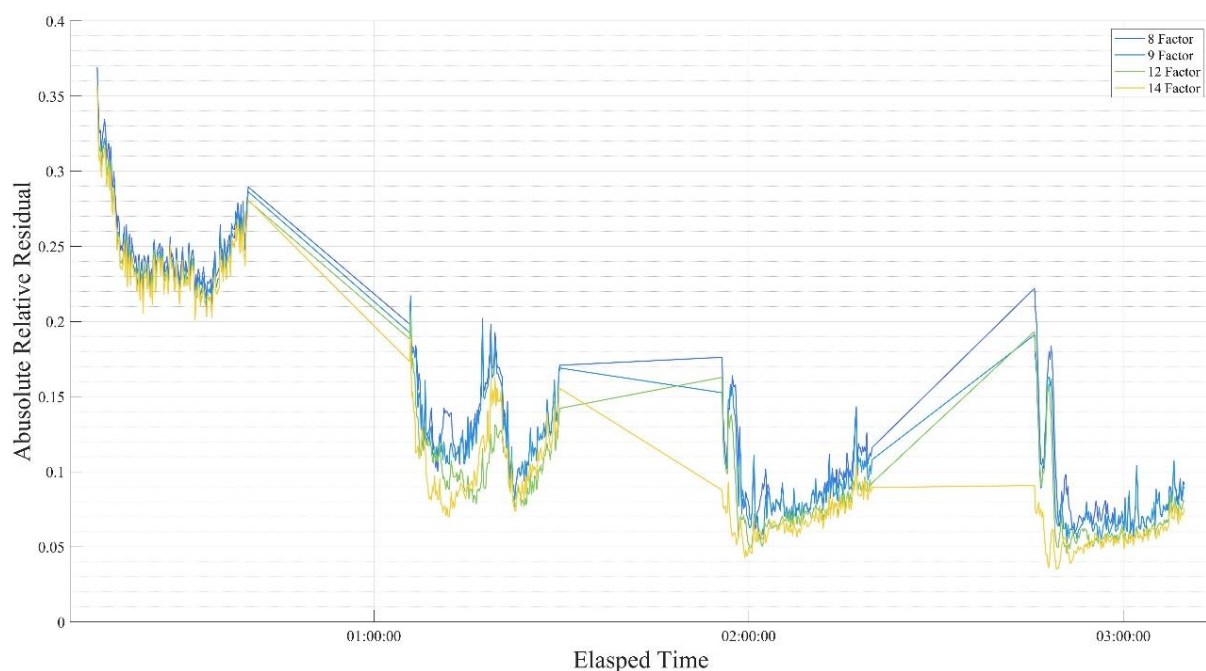
Figure S16 Detailed absolute relative residual time series of factorization results of particle-phase only data utilizing ME-2 PMF with 8,9,12 and 14 factors which are selected to be right at "turning points"
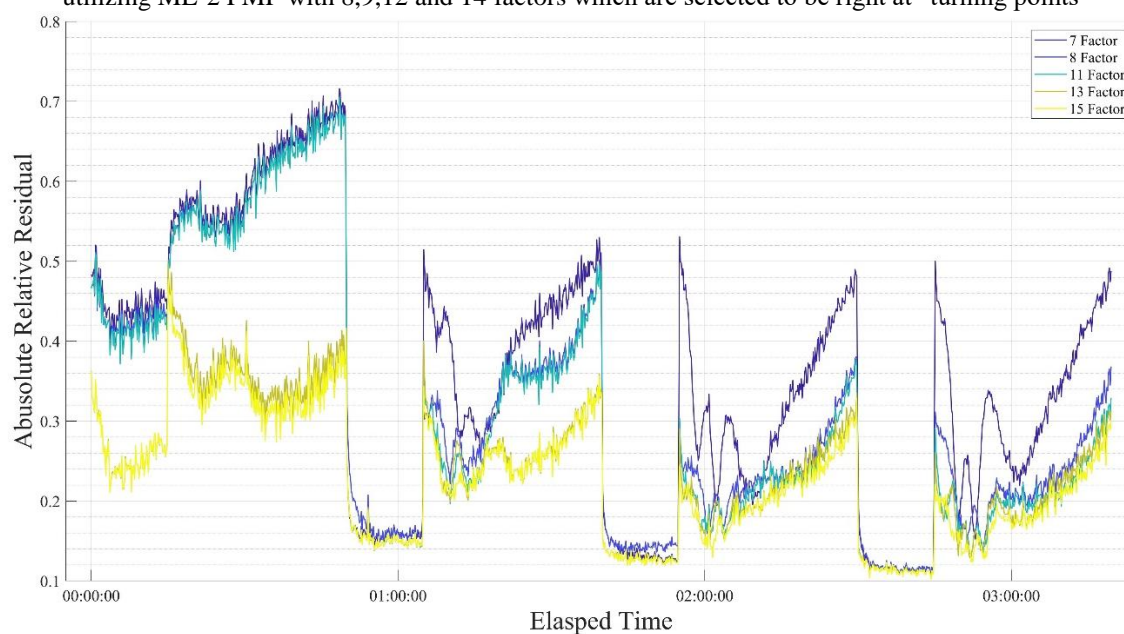
Figure S17 Detailed absolute relative residual time series of factorization results of normalized full time-series data utilizing ME-2 PMF with 7,8,11,13 and 15 factors which are selected to be right at "turning points"
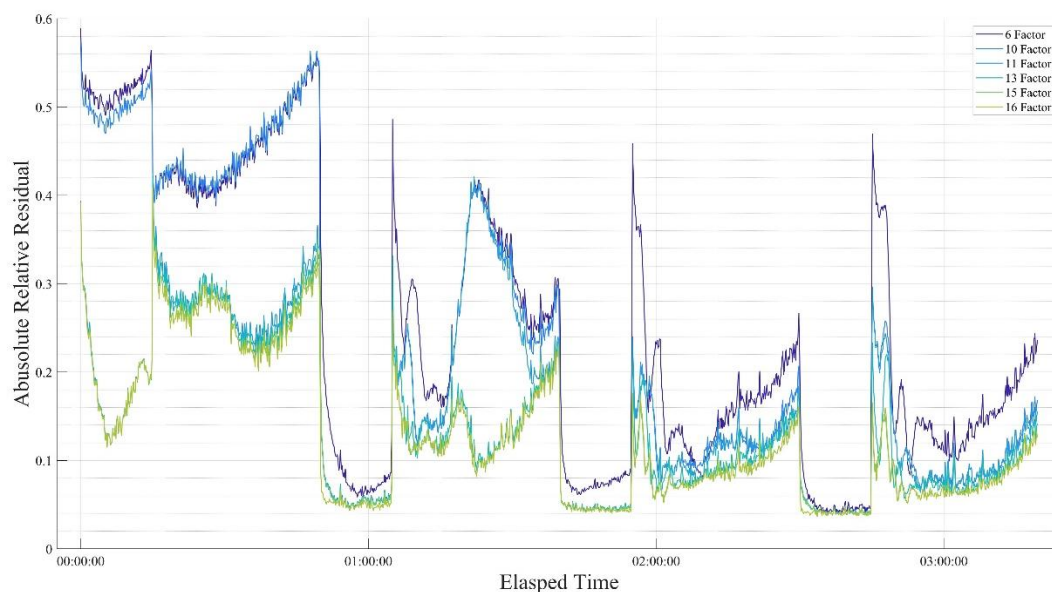
Figure S18 Detailed absolute relative residual time series of factorization results of full time series data utilizing ME-2 PMF with 6,10,11,13,15 and 16 factors which are selected to be right at "turning points"
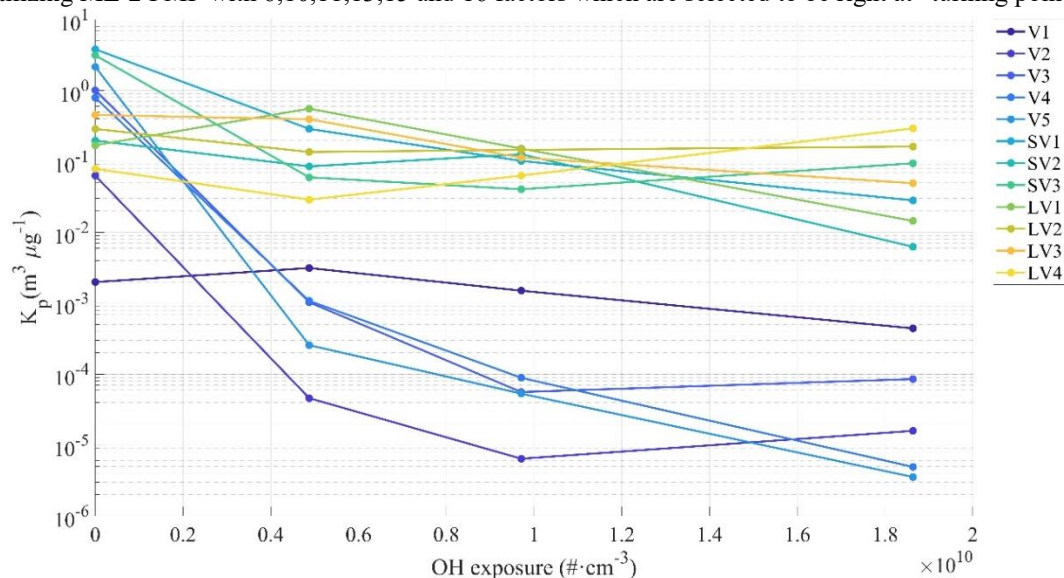
Figure S19 Evolution of factors' gas-particle partitioning coefficient K_p with enhancement of oxidative stage during oxidation process and classification by its volatility

Table S5 Spectra covariance between 13 ME-2 PMF factors represented by contrast angles in degree

	V1	V2	V3	V4	V5	SV1	SV2	SV3	LV1	LV2	LV3	LV4	LV5
V1	0.0	66.0	77.0	70.6	77.4	60.0	83.9	86.9	81.8	81.3	82.9	81.8	86.6
V2	66.0	0.0	65.3	14.2	55.9	75.6	79.0	77.9	77.6	68.9	73.1	71.6	74.9
V3	77.0	65.3	0.0	71.9	44.6	76.0	58.0	63.7	73.1	49.2	57.9	47.2	69.0
V4	70.6	14.2	71.9	0.0	56.2	77.9	78.9	75.4	82.0	71.3	71.9	72.7	72.3
V5	77.4	55.9	44.6	56.2	0.0	73.5	72.7	60.6	81.0	59.0	63.0	53.5	63.5
SV1	60.0	75.6	76.0	77.9	73.5	0.0	81.1	84.7	82.1	75.7	76.7	76.3	83.4
SV2	83.9	79.0	58.0	78.9	72.7	81.1	0.0	48.5	73.2	50.8	33.0	52.1	52.7
SV3	86.9	77.9	63.7	75.4	60.6	84.7	48.5	0.0	77.8	65.0	39.3	49.4	46.3
LV1	81.8	77.6	73.1	82.0	81.0	82.1	73.2	77.8	0.0	74.2	70.4	78.4	79.9
LV2	81.3	68.9	49.2	71.3	59.0	75.7	50.8	65.0	74.2	0.0	40.7	35.7	47.8
LV3	82.9	73.1	57.9	71.9	63.0	76.7	33.0	39.3	70.4	40.7	0.0	39.2	30.9
LV4	81.8	71.6	47.2	72.7	53.5	76.3	52.1	49.4	78.4	35.7	39.2	0.0	49.8
LV5	86.6	74.9	69.0	72.3	63.5	83.4	52.7	46.3	79.9	47.8	30.9	49.8	0.0
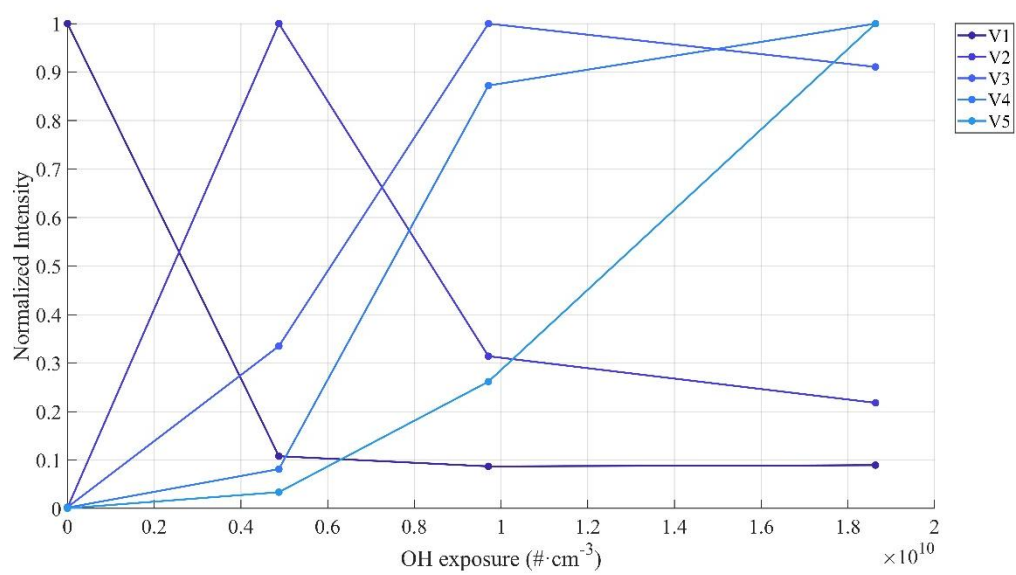
Figure S20
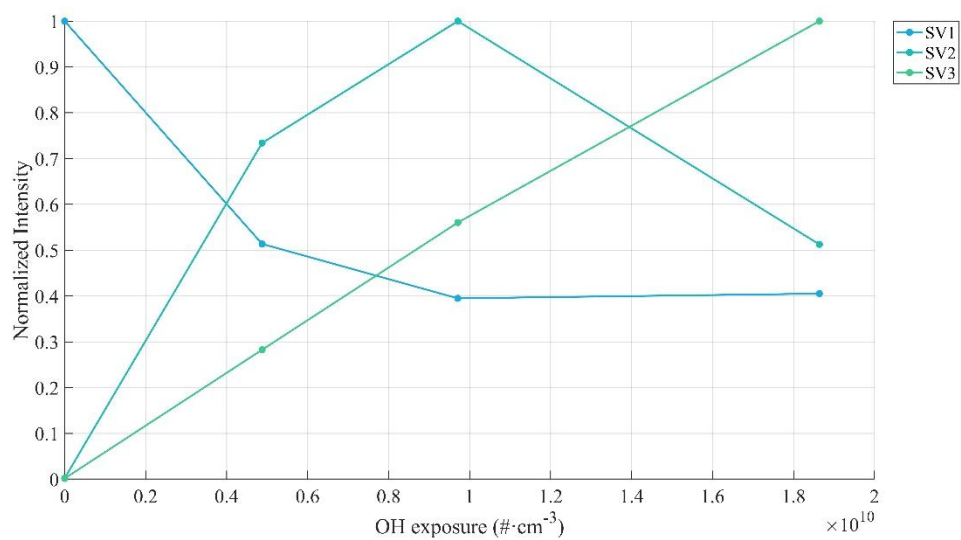
Figure S21
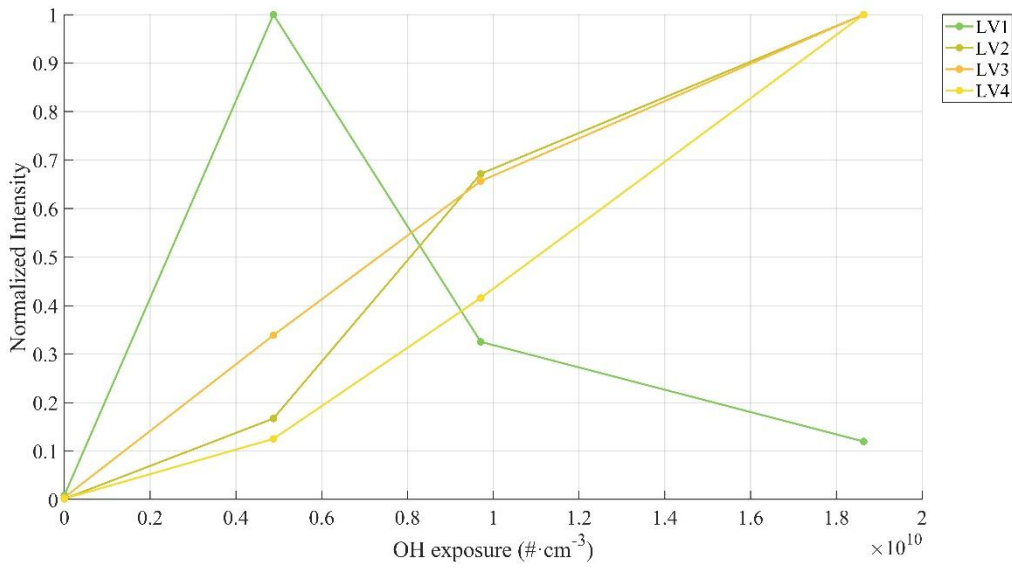
Figure S22

S5. Gas-particle partitioning theme

Volatility and gas-particle partitioning thermodynamics of organic compounds detected by FIAGERO-CIMS are processed by gas-phase and aerosol-phase concentration. Direct gas-particle partitioning characteristics are shown by particle-phase fraction F_p:

$$F_{p,i} = \frac{c_{p,i}}{c_{g,i} + c_{p,i}} \qquad \text{Eq. S13}$$

In Equation S13, $c_{p,i}$ stands for particle phase concentration of substance i, $c_{g,i}$ means gas phase concentration. Partitioning coefficient K_p, considering influence organic aerosol as matrix of substance i, is defined in Equation S14:

$$K_{p,i} = \frac{c_{p,i}/c_p}{c_{g,i}} \qquad \text{Eq. S14}$$

In Equation S14, c_p means total particle concentration. F_p and $K_{p,i}$ can be derived from FIGAERO-CIMS and other corresponding measurement results. detection of certain ion (iodide adduct ion [RI$^-$] or hydrogen extraction ion [R-H]$^-$) corresponding to species R, particle-phase thermal desorption duration and flow rate Δt_{TD} & Q_{TD}, collection duration and flow rate Δt_{col} & Q_{col}, average SMPS-measure particle concentration $c_{p,SMPS}$, shown in Equation S15-S16:

$$(F_{p,i})_{exp} = \frac{\overline{([RI^-]/[I^-])}_{aero} \cdot Q_{TD} \cdot \Delta t_{TD}}{[([RI^-]/[I^-])_{gas} \cdot Q_{col} \cdot \Delta t_{col} + \overline{([RI^-]/[I^-])}_{aero} \cdot Q_{TD} \cdot \Delta t_{TD}]} \qquad \text{Eq. S15}$$

$$(K_{p,i})_{exp} = \frac{\overline{([RI^-]/[I^-])}_{aero} \cdot Q_{TD} \cdot \Delta t_{TD}}{[([RI^-]/[I^-])_{gas} \cdot Q_{col} \cdot \Delta t_{col}] \cdot \overline{c_{p,SMPS}}} \qquad \text{Eq. S16}$$

Eq. S15 and S16 can be used to classify PMF factor from volatility angle by substituting intensity of certain compound [RI$^-$]/[I$^-$] with intensity of one factor. Gas-particle partitioning in POA and SOA mainly follows absorption mechanism[25, 26],where species exist in aerosol phase at liquid-solution state. Considering the mechanism of absorption partitioning, F$_p$ is related to mass of total particle phase organics c$_{OM}$, shown in Equation S17[27], while K$_P$ only depends on properties of species i and particle phase composition. Assuming gas-particle partitioning of component i reaches its equilibrium, partitioning coefficient K$_{p,i}$ is determined by organic aerosol composition and volatility of compound i as shown in Equation S18:

$$(F_{p,i})_{theo} = \left(1 + \frac{c^*}{c_{OM}}\right)^{-1} \qquad \text{Eq. S17}$$

$$(K_{p,i})_{theo} = \frac{RTf_{OM}}{MW_{OM}p^0_{L,i}\xi_i} \qquad \text{Eq. S18}$$

In Eq. S18, f$_{OM}$ means fraction of organic part in aerosols, which is set to 1 in this study. MW$_{OM}$ stands for mean molecular weight among all species in organic aerosol. p$^0_{L,i}$ means saturated vapor pressure of component i over liquid pure component surface. ξ_i means activity coefficient in particle phase. Assuming ξ_i as close to unity, the volatility of component i can be determined from gas-particle partitioning of component. If we are able to classify the exact structure from possible reaction path during oxidation of utilize estimation method of volatility from corresponding compound detected by CIMS such as SIMPOL & EVAPORATION[28, 29] .We could also adopt 2-D VBS approach listed in Section S3 to calculate volatility of certain species, which may lead to larger bias. Volatility of species i can be also determined by thermogram from thermal desorption measurements of particle phase according to methods mentioned in section S2[30, 31], which may be more accurate than partitioning method due to possible interference such as thermal desorption[32]. After the volatility has been obtained, activity coefficient ξ_i can be briefly determined so as to account for composition influence on gas-particle partitioning and possible kinetic effects.

Gas-particle partitioning of organic species may not reach equilibrium because of kinetic limitations. Gas-particle partitioning kinetics consist of gas phase diffusion, surface accommodation and particle-phase diffusion processes, the kinetics are determined by gas-phase diffusion coefficient D$_{g,i}$, surface accommodation coefficient α, and particle-phase diffusion coefficient D$_{p,i}$. Gas phase diffusion coefficient of species i in real atmosphere can be calculated from elemental composition of selected species from Fuller's method:

$$D_{g,i} = \frac{1.0868 \times T^{1.75}}{p \cdot \sqrt[3]{m(i,A)} \cdot (\sqrt[3]{V_A} + \sqrt[3]{V_i})^2}$$ Eq. S19

In equation S19, $D_{g,i}$ is in cm^2 s^{-1}, T and p is atmospheric temperature and pressure in Kelvin and Torr, $m(i,A)$ means reduced molar mass of species i and ambient air in g/mol, V_i and V_A are molecular diffusion volume of ambient air and selected species i, which can be directly estimated by elemental composition. Most organic species involved in gas-particle partitioning have diffusion coefficient within 10^{-2} to 10^{-1} cm^2 s^{-1} level[33]. Particle phase diffusion $D_{p,i}$ are connected particle phase viscosity ν, shown in Equation S20 (Stokes-Einstein Equation)[34]:

$$D_{p,i} = \frac{kT}{6\pi a \nu}$$ Eq. S20

In Eq. S20, k is Boltzmann constant, T is particle-phase temperature, a means effective molecular diameter in molecular diffusion, which are at the level of several Å[35, 36]. Particle-phase viscosity can be parameterized by composition distribution in 2-D VBS space that has been detailed discussed [37]. Gas-particle partitioning kinetic can thus be estimated by time scale of gas-phase diffusion and particle-phase diffusion. Gas-phase and particle-phase diffusion characteristic time scale $\tau_{g,i}$ and $\tau_{p,i}$ are shown in Equations S21-S25[34, 38]:

$$\tau_{g,i} = 1/k_{gp,i}$$ Eq. S21

$$k_{gp,i} = \sum_p 4\pi D_{g,i} r_p N_p \beta$$ Eq. S22

$$\beta = \frac{0.75\alpha(1+Kn)}{Kn^2 + Kn + 0.283Kn\alpha + 0.75\alpha}$$ Eq. S23

$$Kn = \frac{3D_{g,i}}{\omega r_p}$$ Eq. S24

$$\tau_{p,i} = \frac{d_p^2}{4\pi^2 D_{p,i}}$$ Eq. S25

In Equations S21-S25, r_p is particle radius, d_p is diameter and N_p is particle number concentration at certain diameter range, measured by SMPS; β is correction factor adjusting surface accommodation related to Knudsen number Kn, ω is mean thermal velocity of species i. Comparison between $\tau_{g,i}$, $\tau_{p,i}$ and retention time in Go:PAM t_R(55s) give us insight into gas-particle partitioning dynamics in the experiment.

S6. Additional results
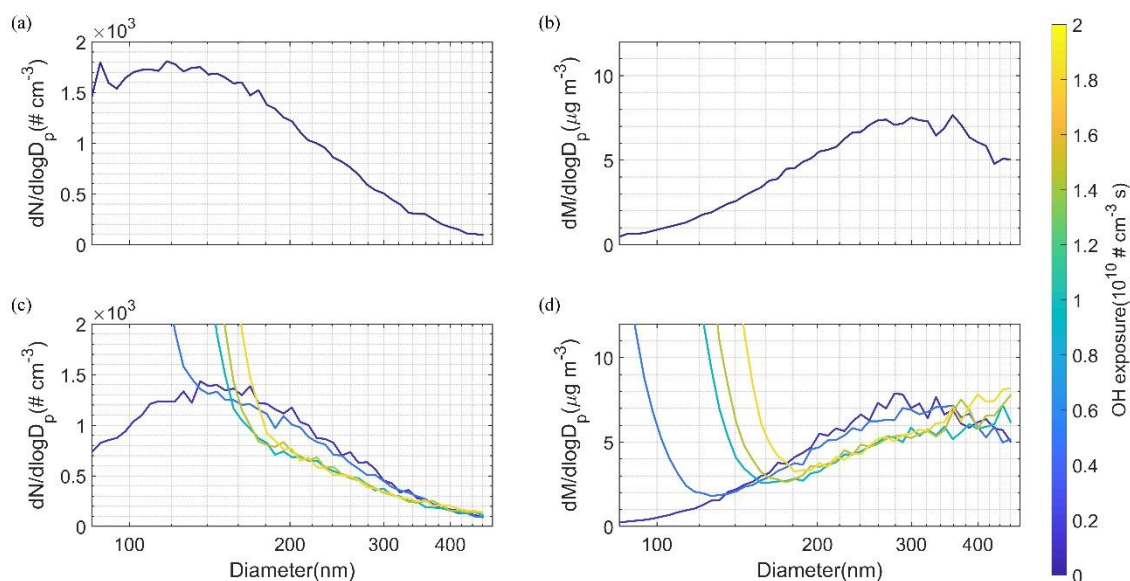
Figure S23 Primary and secondary aerosol size & mass distribution evolution at diameter>90nm while oxidation age increase. (a) stands for number distribution, (b) mass distribution of primary particles, (c) (d) number distribution & mass distribution of secondary aerosols in Go:PAM flow tube at OH radical exposure $0.1\sim1.8\times10^{10}$ cm^{-3} s
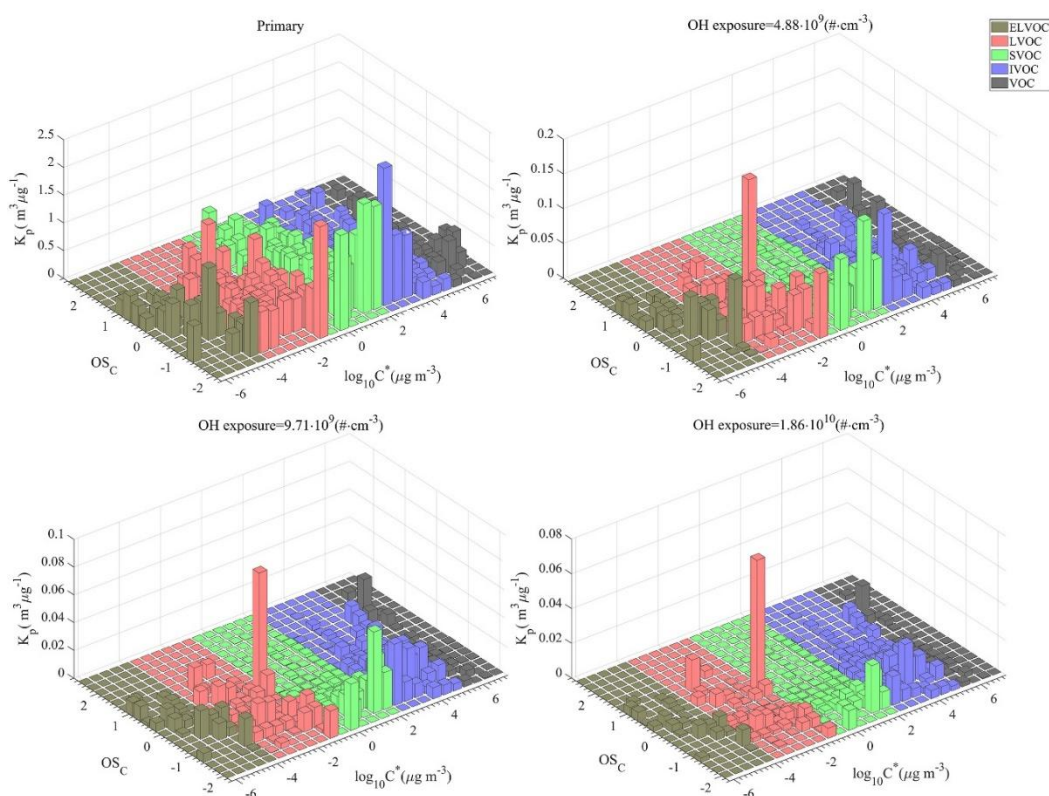
Figure S24 Distribution of primary& secondary cooking aerosols' partitioning coefficient K_p between gas-phase and particle-phase in 2-D VBS space

Table S6 Size and mass distribution parameters & quantities of primary and secondary cooking aerosol

OH radical exposure (10^{10} cm^{-3}·s)	OA Mass concentration (μg·m^{-3})	Size distribution mode diameter(nm)	Mass distribution mode diameter(nm)	Density (g·cm^{-3})
Primary	3.36	-*	-*	1.00*
		113.4**	289**	1.05**
0.112	10.5	14.1*	27.9*	1.02*
		151.2**	279**	1.09**
0.488	42.8	21.7*	46.1*	1.03*
		-**	-**	1.09**
0.971	87.0	27.9*	53.3*	1.02*
		-**	-**	1.10**
1.48	107	28.9*	55.2*	1.06*
		-**	-**	1.11**
1.86	144	31.1*	61.5*	1.08*
		-**	-**	1.13**

* Particle size below 100nm, related to secondary aerosol formed from primary vapor oxidation and then OM vapor nucleation and growth

**Particle size over 100nm, related to primary aerosol and condensation
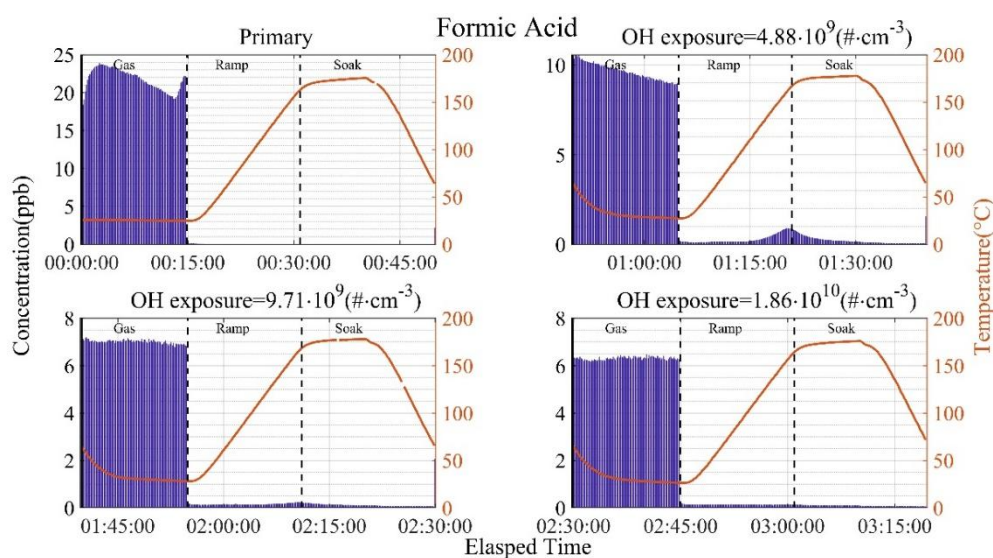
Figure S25 Time series of formic acid concentration at different oxidative state during FIAGERO measurement of flow tube experiment. Concentration of **formic acid and following species** is converted from signal intensity utilizing methods in section S2.
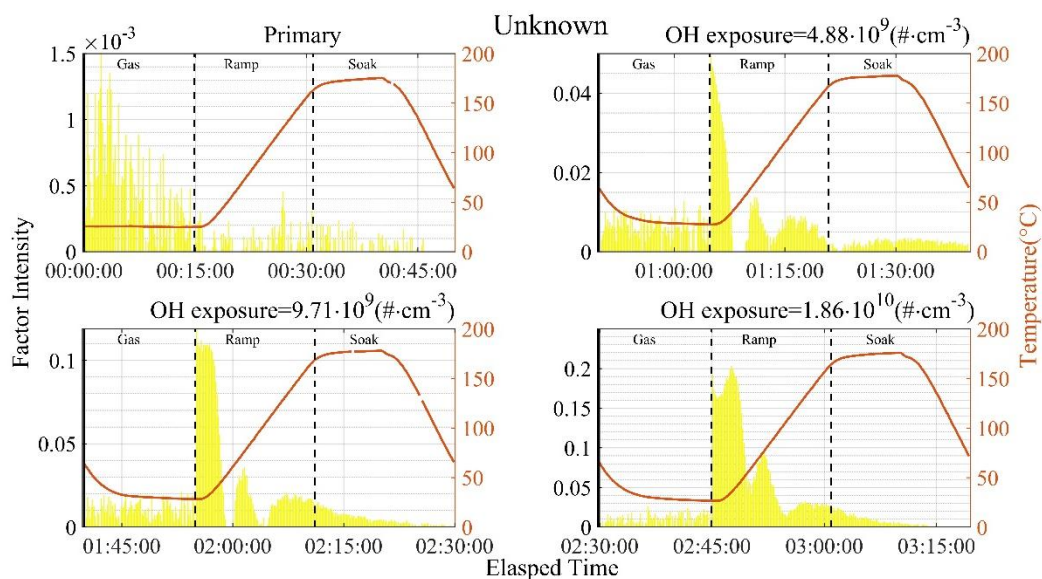
Figure S26 Intensity time series of contaminant factor Unknown in PMF results at different oxidative stage during FIAGERO measurement circles

Table S7 Average composition and top-20 most abundant species in Factor V1 from ME-2 PMF results

Factor Name: Factor V1			
Average elemental composition: $C_{3.20}H_{5.23}O_{2.71}N_{0.01}S_{0.01}$ MW=87.27 OS_c=0.148			
20 most abundant compounds in molecular composition:			
Molecules	Intensity	MW(g·mol^{-1})	Possible species
$C_2H_4O_2$	0.79	60.02	Acetic acid
$C_3H_4O_2$	0.58	72.02	Acrylic acid
$C_5H_4O_4$	0.094	128.01	Hydroxy furoic acid
$C_5H_{10}O_6$	0.089	166.04	Arabic acid
$C_3H_6O_4$	0.083	106.03	Glyceric acid
$C_2H_4O_4$	0.081	92.01	Hydroperoxy acetic acid
$C_3H_4O_3$	0.044	88.02	Pyruvic acid
$C_6H_{12}O_2$	0.037	116.08	Hexanoic acid
$C_3H_6O_3$	0.029	90.03	Lactic acid
$C_6H_{10}O_3$	0.028	130.06	Oxo-hexanoic Acid
$C_4H_6O_4$	0.023	118.03	Succinic acid
$C_2H_4O_3$	0.022	76.02	Glycolic acid
$C_5H_8O_3$	0.020	116.04	Oxopentanoic acid
$C_6H_{12}O_3$	0.020	132.07	Hydroxy hexanoic acid
$C_3H_4O_4$	0.016	104.01	Malonic acid
$C_2H_2O_4$	0.016	89.99	Oxalic acid
$C_3H_8O_3$	0.016	92.05	glycerol
$C_4H_4O_3$	0.014	100.02	Oxo-butenoic acid
$C_4H_4O_4$	0.0085	116.01	Fumaric acid
$C_5H_{10}O_3$	0.0082	118.06	2-Oxo-Pentanoic acid

Table S8 Average composition and top-20 most abundant species in Factor SV1 from ME-2 PMF results

Factor Name: Factor SV1
Average elemental composition: $C_{5.00}H_{7.12}O_{3.80}N_{0.01}S_{0.01}$ MW=128.25 OS_C=0.402

Molecular composition:			
Molecules	Intensity	MW(g·mol⁻¹)	Possible species
$C_5H_4O_4$	0.84	128.01	Hydroxy furoic acid
$C_2H_2O_4$	0.28	90.00	Oxalic acid
$C_3H_6O_3$	0.23	90.03	Lactic acid
$C_2H_4O_3$	0.14	76.02	Glycolic acid
$C_6H_{10}O_3$	0.14	130.06	Oxo-hexanoic Acid
$C_2H_4O_2$	0.14	60.02	Acetic acid
$C_3H_4O_4$	0.14	104.01	Malonic acid
$C_5H_8O_3$	0.13	116.05	Oxo-pentatonic acid
$C_3H_4O_3$	0.11	88.02	Pyruvic acid
$C_5H_8O_6$	0.088	164.03	Dihydroxy glutaric acid
$C_6H_{10}O_5$	0.085	162.05	Hydroxy adipic acid
$C_6H_{12}O_3$	0.084	132.08	Hydroxy hexanoic acid
$C_4H_6O_4$	0.081	118.03	Succinic acid
$C_6H_{10}O_4$	0.062	146.06	Adipic acid
$C_5H_8O_4$	0.060	132.04	Glutaric acid
$C_3H_8O_3$	0.051	92.05	Glycerol
$C_3H_6O_4$	0.043	106.03	Glyceric acid
$C_5H_{10}O_3$	0.036	118.06	Hydroxy valeric acid
$C_5H_6O_5$	0.036	146.02	Ketoglutaric acid
$C_9H_{16}O_4$	0.035	188.10	Azelaic acid

Figure S27 Intensity time series of volatile primary emission factor V1 (presented remarkably only in gas phase) in PMF results at different oxidative stage during FIAGERO measurement circles.
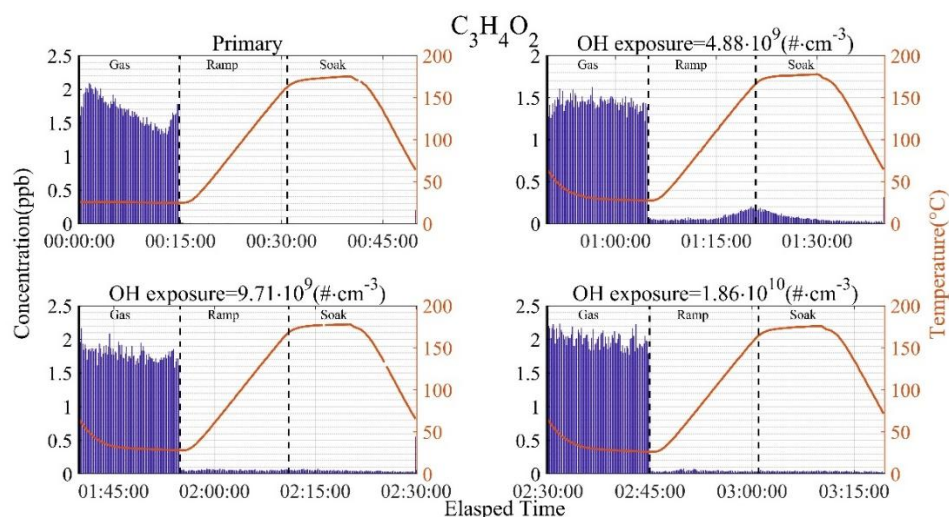
Figure S28 Concentration time series of compound with elemental composition of $C_3H_4O_2$ (probably acrylic acid, representing volatile primary organics from thermal decomposition of glycerol) at different oxidative stage during FIAGERO measurement of flow tube experiment.
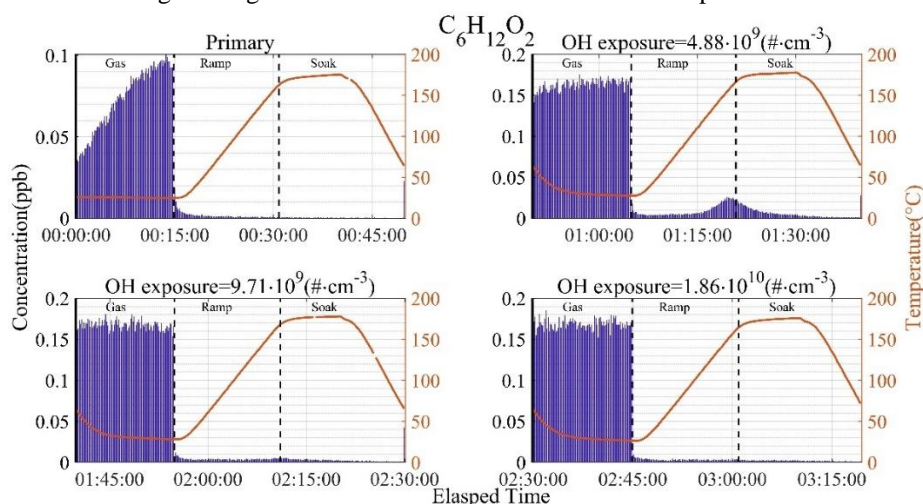
Figure S29 Concentration time series of compound with elemental composition of $C_6H_{12}O_2$ (probably hexanoic acid, representing volatile primary organics majority from thermal oxidation of primary long-chain aliphatic acids, minority from photo-oxidation) at different oxidative stage during FIAGERO measurement of flow tube experiment.
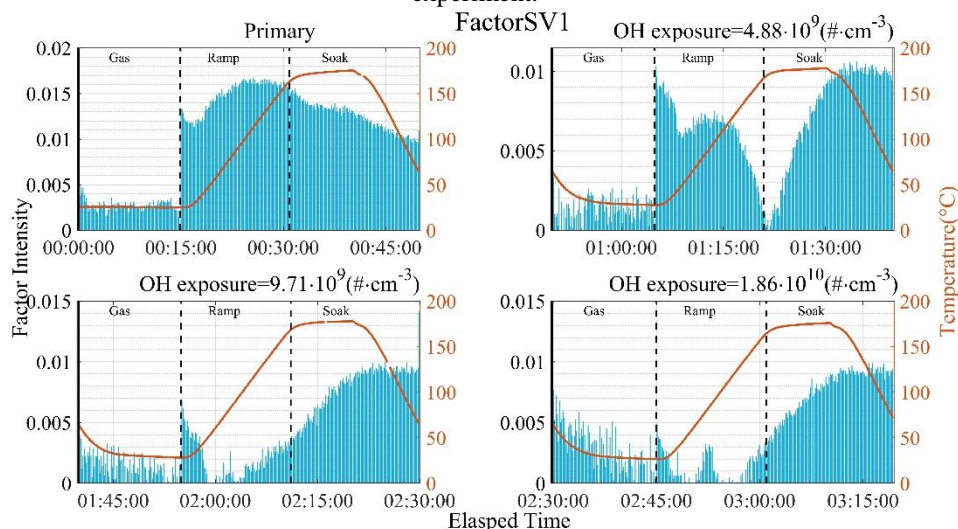
Figure S30 Intensity time series of semi-volatile primary emission factor SV1 (presented remarkably in both gas phase and aerosol phase) in PMF results at different oxidative stage during FIAGERO measurement circles.
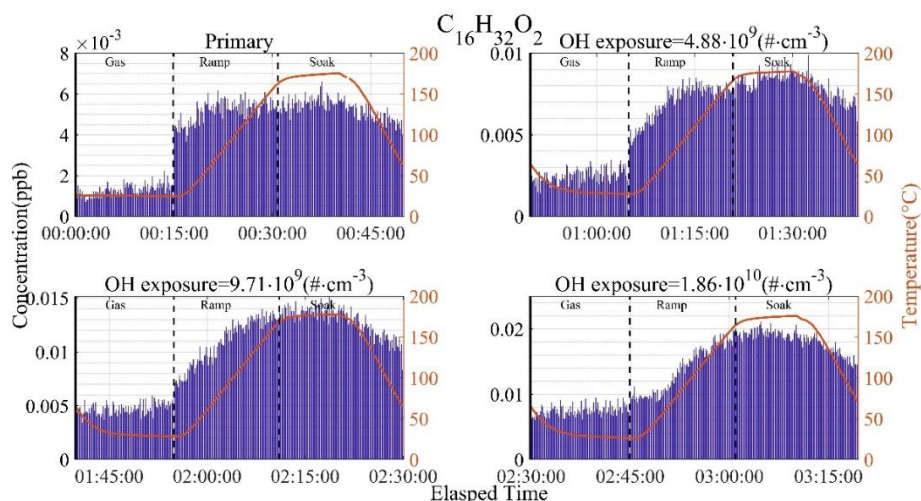
Figure S31 Concentration time series of compound with elemental composition of $C_{16}H_{32}O_2$ (probably Palmitic acid, representing long-chain saturated carboxylic acids as semi-volatile primary markers of cooking emission) at different oxidative stage during FIAGERO measurement of flow tube experiment.
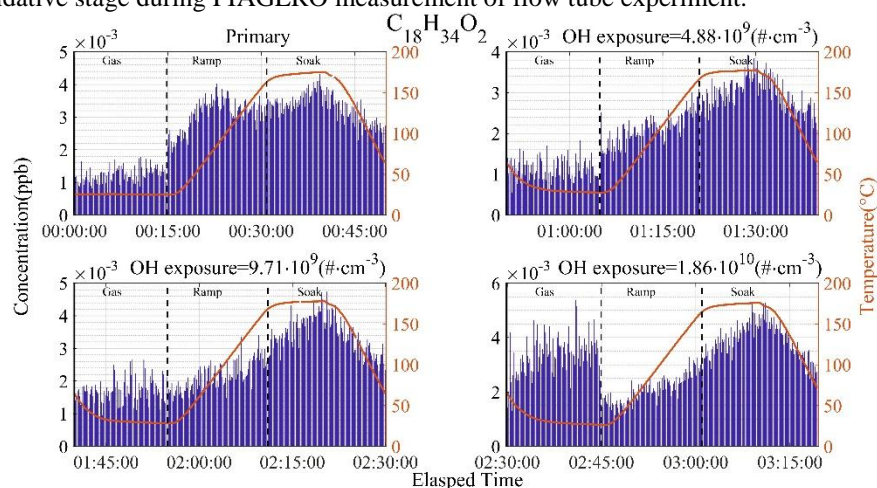
Figure S32 Concentration time series of compound with elemental composition of $C_{18}H_{34}O_2$ (probably Oleic acid, representing long-chain unsaturated acids as semi-volatile primary markers of cooking emission) at different oxidative stage during FIAGERO measurement of flow tube experiment.
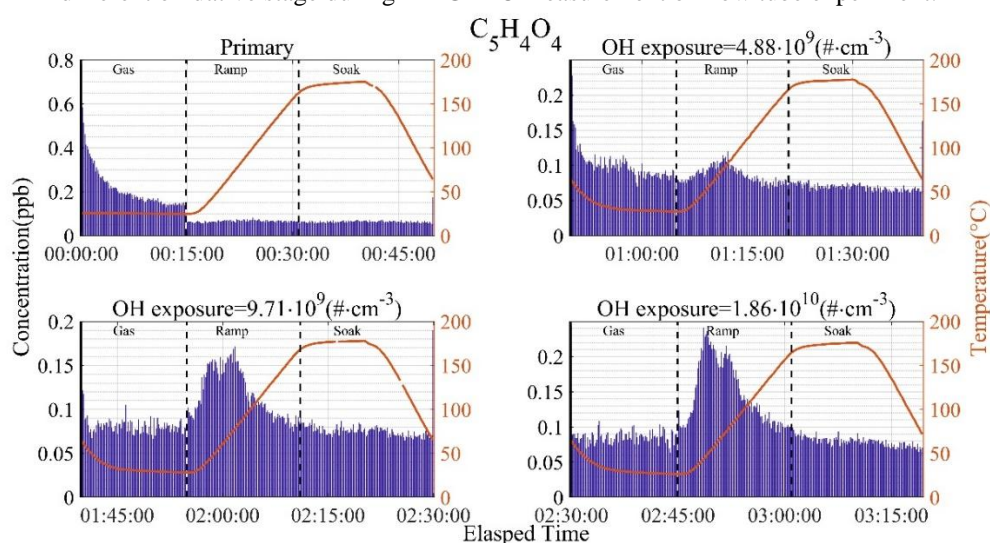
Figure S33 Concentration time series of compound with elemental composition of $C_5H_4O_4$ (possibly aconic acid or hydroxy furoic acid, representing primary emissions from thermal oxidation and decomposition) at different oxidative stage during FIAGERO measurement of flow tube experiment.
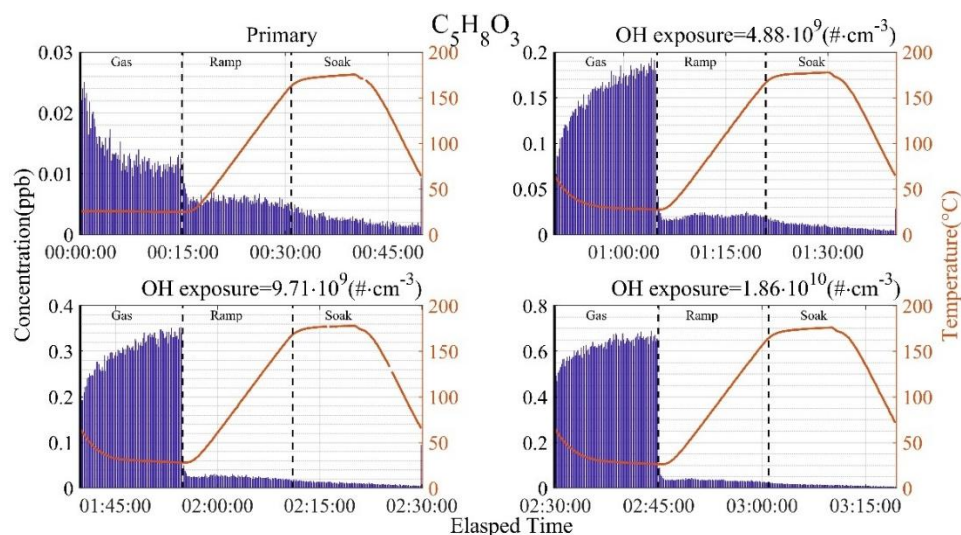
Figure S34 Concentration time series of compound with elemental composition of $C_5H_8O_3$ (possibly oxo-pentatonic acids) at different oxidative stage during FIAGERO measurement of flow tube experiment.
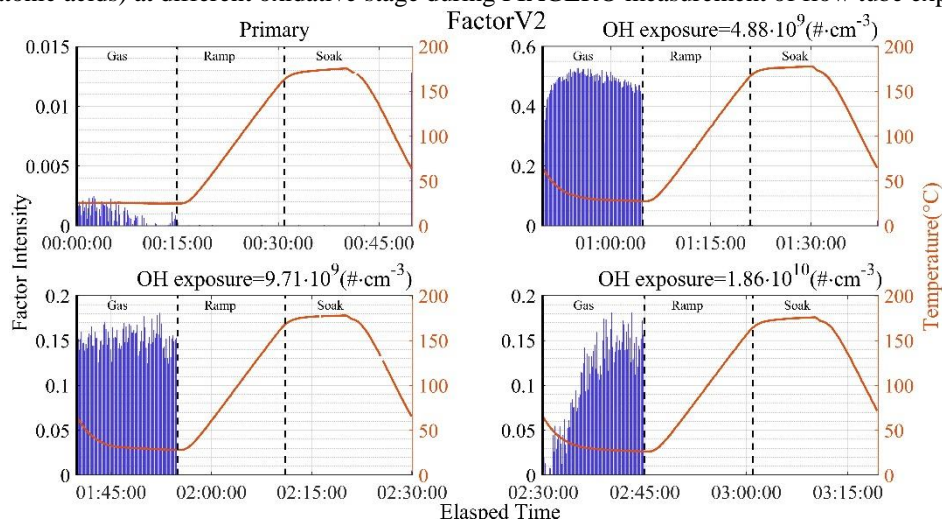
Figure S35 Intensity time series of volatile intermediate oxidative state factor V2 (presented remarkably only in gas phase) in PMF results at different oxidative stage during FIAGERO measurement circles.
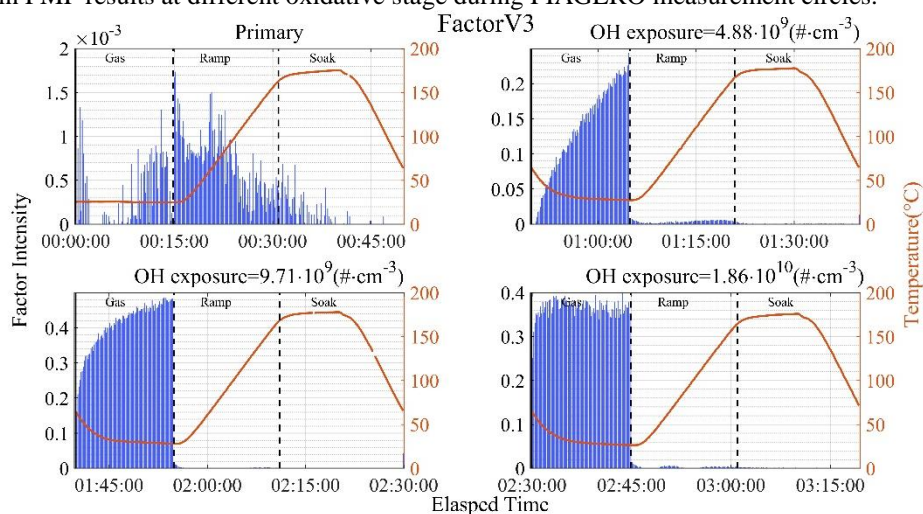
Figure S36 Intensity time series of volatile intermediate oxidative state factor V3 (abundant most in gas phase) in PMF results at different oxidative stage during FIAGERO measurement circles.
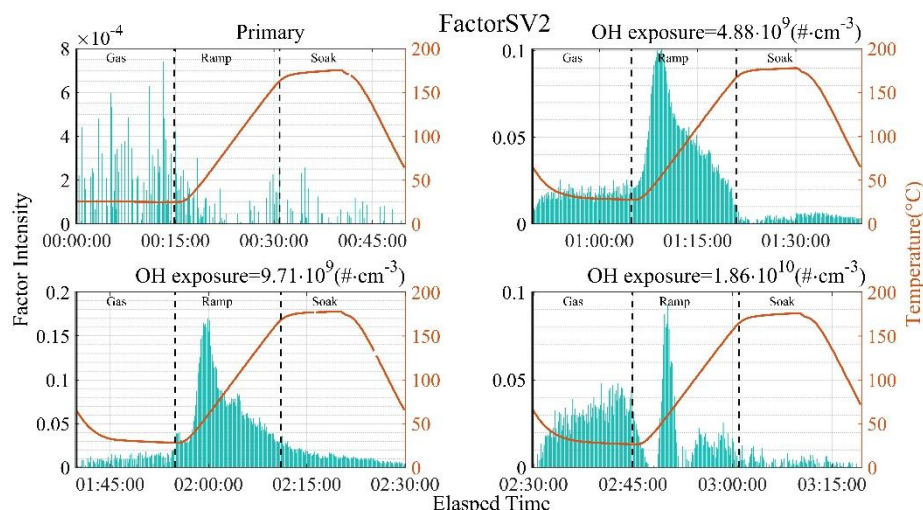
Figure S37 Intensity time series of semi-volatile intermediate oxidative state factor Factor SV2 (abundant both in gas phase and aerosol phase) in PMF results at different oxidative stage during FIAGERO measurement circles.
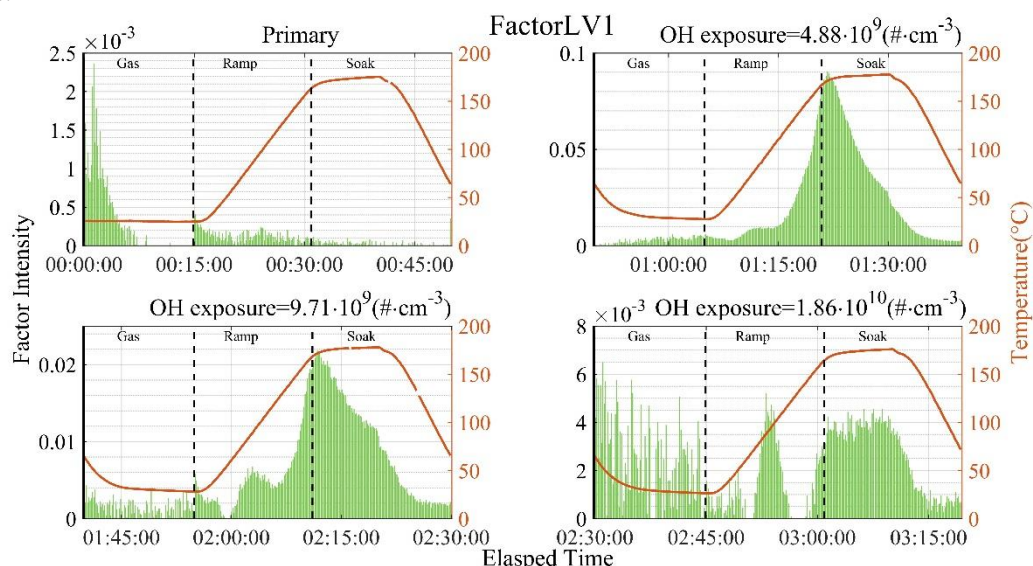
Figure S38 Intensity time series of semi-volatile intermediate oxidation product factor Factor LV1 (abundant most in aerosol phase) in PMF results at different oxidative stage during FIAGERO measurement circles.

Table S9 Average composition and top-20 most abundant species in Factor V2 from ME-2 PMF results

Factor Name: Factor V2			
Average elemental composition: $C_{4.68}H_{7.92}O_{3.81}N_{0.03}S_{0.05}$ MW=126.87 OS_C=0.405			
Molecular composition:			
Molecules	MW(g·mol^{-1})	Relative Intensity	Possible species
$C_2H_4O_4$	92.01096	0.69566	Hydroperoxy acetic acid
$C_3H_4O_4$	104.011	0.291804	Malonic acid
$C_7H_{12}O_4$	160.0736	0.237051	Pimelic acid
$C_3H_4O_3$	88.0155	0.224047	Pyruvic acid
$C_2H_2O_4$	89.99531	0.21201	Oxalic acid
$C_2H_4O_2$	60.02113	0.201705	Acetic acid
$C_7H_{12}O_5$	176.0685	0.18606	Hydroxy pimelic acid
$C_6H_{10}O_3$	130.063	0.171717	Oxo-hexanoic Acid
$C_7H_{14}O_4$	162.0887	0.152692	Dihydroxy heptanoic acid

$C_6H_{10}O_4$	146.0579	0.147952	Adipic acid
$C_6H_{12}O_3$	132.0786	0.141303	Hydroxy hexanoic Acid
$C_3H_4O_2$	72.02113	0.136328	Acrylic acid
$C_4H_4O_3$	100.016	0.128605	Oxo-butenoic acid
$C_3H_6O_4$	106.0266	0.116571	Glyceric acid
$C_6H_{12}O_4$	148.0736	0.09489	Dihydroxy hexanoic Acid
CH_2O_3	61.99985	0.065981	-
$C_4H_6O_5$	134.021	0.063952	Malic acid
$C_5H_8O_3$	116.0468	0.061708	Oxo-pentatonic acid
$C_3H_6S_2$	105.9911	0.060226	-
$C_5H_6O_5$	146.0215	0.056191	Oxo glutaric acid

Table S10 Average composition and top-20 most abundant species in Factor V3 from ME-2 PMF results

Factor Name: Factor V3

Average elemental composition:

$C_{6.49}H_{10.94}O_{3.96}N_{0.01}S_{0.01}$

MW=152.86 OS_C=-0.281

Molecular composition:

Molecules	MW(g·mol^{-1})	Relative Intensity	Possible species
$C_6H_{12}O_3$	132.0786	0.516467	Hydroxy hexanoic Acid
$C_6H_{10}O_3$	130.063	0.400322	Oxo-hexanoic Acid
$C_7H_{12}O_5$	176.0685	0.337381	Hydroxy pimelic acid
$C_4H_4O_3$	100.016	0.28861	Oxo-butenoic acid
$C_6H_{10}O_4$	146.0579	0.232466	Adipic acid
$C_2H_4O_2$	60.02113	0.19557	Acetic acid
$C_3H_4O_4$	104.011	0.191313	Malonic acid
$C_7H_{12}O_4$	160.0736	0.182699	Pimelic acid
$C_3H_4O_3$	88.0155	0.177969	Pyruvic acid
$C_7H_{14}O_5$	178.0841	0.132052	Hydroxy hydroperoxyl heptanoic acid
$C_{10}H_{16}O_3$	184.1099	0.128191	Oxo-decanoic acid
$C_9H_{16}O_4$	188.1049	0.113297	Azelaic acid
$C_6H_{12}O_4$	148.0736	0.109202	Dihydroxy hexanoic Acid
$C_7H_{12}O_6$	192.0634	0.109095	Hydroperoxy pimelic acid
$C_3H_4O_2$	72.02113	0.108079	Acrylic acid
$C_5H_8O_3$	116.0468	0.099506	Oxo-pentatonic acid
$C_5H_6O_5$	146.0215	0.095848	Oxo glutaric acid
$C_7H_{12}O_3$	144.0786	0.074596	Hydroxy heptanoic acid
$C_5H_{10}O_3$	118.0624	0.069336	2-Oxo-Pentanoic acid
$C_{10}H_{16}O_6$	232.0941	0.060075	Decanetrioic acid

Table S11 Average composition and top-20 most abundant species in Factor SV2 from ME-2 PMF results

Factor Name: Factor SV2

Average elemental composition:

$C_{7.69}H_{13.72}O_{3.88}N_{0.00}S_{0.00}$

MW=168.29 OS_C=-0.662

Molecular composition:

Molecules	MW(g·mol^{-1})	Relative Intensity	Possible species
$C_9H_{16}O_4$	188.1049	0.505217	Azelaic acid
$C_9H_{18}O_4$	190.1205	0.44474	Hydroperoxyl nonanoic acid
$C_6H_{12}O_4$	148.0736	0.404834	Hydroperoxyl hexanoic acid
$C_{10}H_{18}O_4$	202.1205	0.394289	Sebacic acid

Molecules	MW	Relative Intensity	Possible species
$C_6H_{12}O_3$	132.0786	0.209654	Hydroxyl hexanoic acid
$C_6H_{10}O_4$	146.0579	0.162467	Adipic acid
$C_{10}H_{16}O_3$	184.1099	0.147793	Oxo-decanoic acid
$C_3H_4O_3$	88.0155	0.137486	Pyruvic acid
$C_7H_{12}O_4$	160.0736	0.13194	Pimelic acid
$C_6H_{10}O_3$	130.063	0.129637	Oxo-hexanoic Acid
$C_9H_{14}O_4$	186.0892	0.121187	Nonendioic acid
$C_9H_{16}O_5$	204.0998	0.100231	Hydroxy azelaic acid
$C_{10}H_{18}O_3$	186.1256	0.089287	Oxodecanoic acid
$C_{10}H_{16}O_4$	200.1049	0.073579	Decendioic acid
$C_9H_{16}O_3$	172.1099	0.066601	Oxo-nonanoic acid
$C_7H_{12}O_5$	176.0685	0.063406	Hydroxy pimelic acid
$C_3H_4O_4$	104.011	0.060367	Malonic acid
$C_4H_4O_3$	100.016	0.054027	Oxo-butenoic acid
$C_7H_{14}O_5$	178.0841	0.049281	Hydroxy hydroperoxyl heptanoic acid
$C_8H_{18}O_4$	178.1205	0.048359	Hydroperoxy Octanediol

Table S12 Average composition and top-20 most abundant species in Factor LV1 from ME-2 PMF results

Factor Name: Factor LV1

Average elemental composition:
$C_{4.67}H_{7.37}O_{3.50}N_{0.00}S_{0.00}$
MW=119.59 OS$_C$=0.300

Molecular composition:

Molecules	MW(g·mol^{-1})	Relative Intensity	Possible species
$C_3H_4O_3$	88.0155	0.920802	Pyruvic acid
$C_3H_4O_4$	104.011	0.329353	Malonic acid
$C_9H_{16}O_5$	204.0998	0.1666	Hydroxy azelaic acid
$C_6H_{12}O_3$	132.0786	0.062601	Hydroxy hexanoic acid
$C_9H_{16}O_4$	188.1049	0.049186	Azelaic acid
$C_6H_{10}O_4$	146.0579	0.039255	Adipic acid
$C_3H_4O_2$	72.02113	0.034696	Acrylic acid
$C_{10}H_{16}O_3$	184.1099	0.03121	Oxo-decanoic acid
$C_6H_{10}O_3$	130.063	0.028194	Oxo-hexanoic Acid
$C_9H_{18}O_4$	190.1205	0.026098	Hydroperoxyl nonanoic acid
$C_{10}H_{18}O_4$	202.1205	0.024655	Sebacic acid
$C_7H_{12}O_4$	160.0736	0.023498	Pimelic acid
$C_5H_4O_4$	128.011	0.021765	Hydroxy furoic acid
$C_6H_{12}O_4$	148.0736	0.021387	Dihydroxy hexanoic Acid
$C_2H_4O_2$	60.02113	0.016833	Acetic acid
$C_9H_{14}O_4$	186.0892	0.015728	Nonendioic acid
$C_5H_8O_3$	116.0468	0.014809	Oxo-pentanoic acid
$C_4H_4O_3$	100.016	0.013434	Oxo-butenoic acid
$C_9H_{16}O_3$	172.1099	0.013015	Oxo-nonanoic acid
$C_{10}H_{18}O_3$	186.1256	0.011866	Oxo-decanoic acid
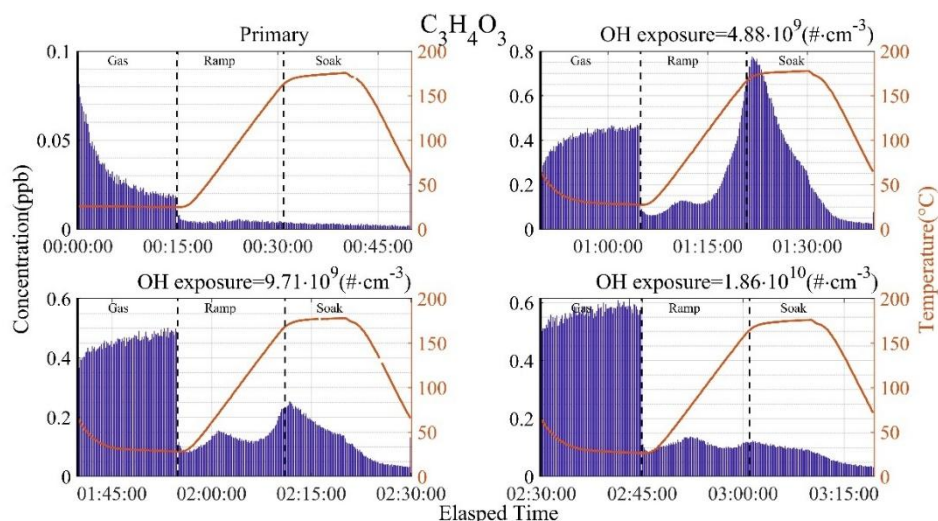
Figure S39 Concentration time series of compound with elemental composition of $C_3H_4O_3$ (probably pyruvic acid) at different oxidative stage during FIAGERO measurement of flow tube experiment.
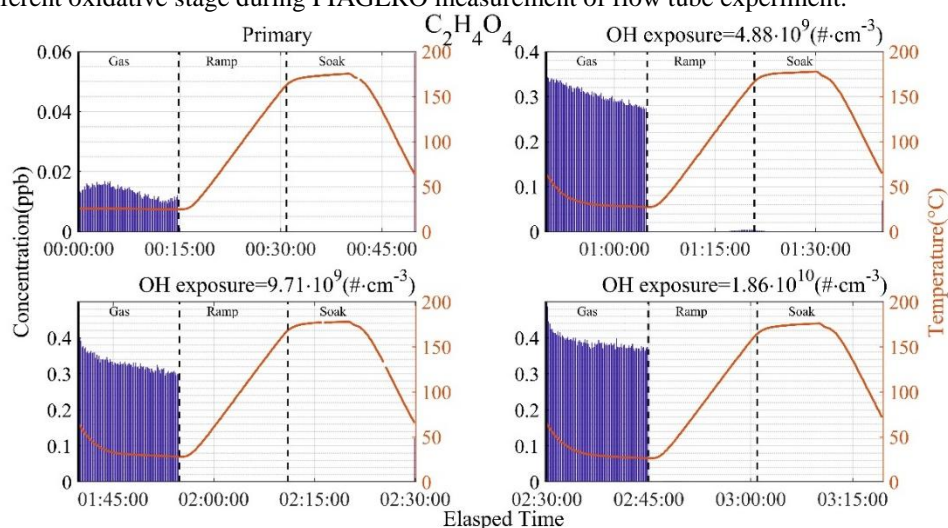
Figure S40 Concentration time series of compound with elemental composition of $C_2H_4O_4$ (possibly hydroperoxyl acetic acid) at different oxidative stage during FIAGERO measurement of flow tube experiment.
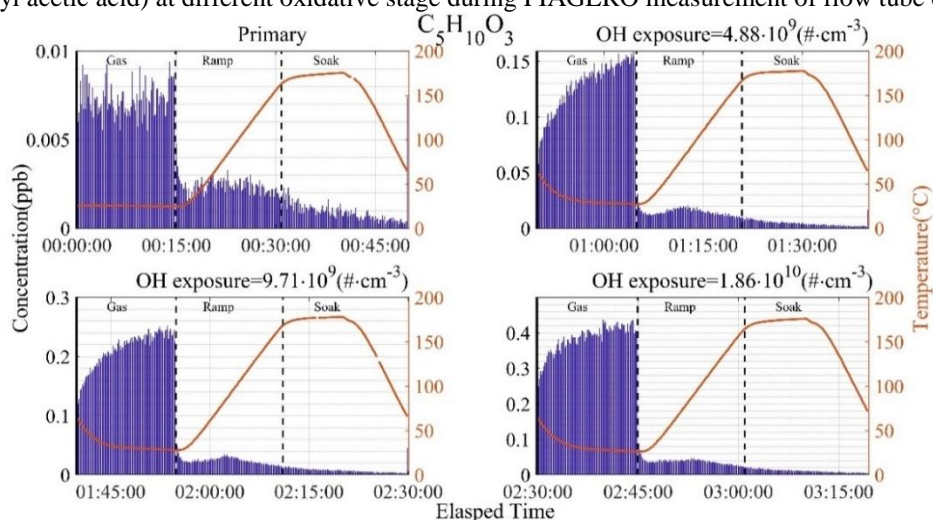
Figure S41 Concentration time series of compound with elemental composition of $C_5H_{10}O_3$ (possibly oxo-pentatonic acids) at different oxidative stage during FIAGERO measurement of flow tube experiment.
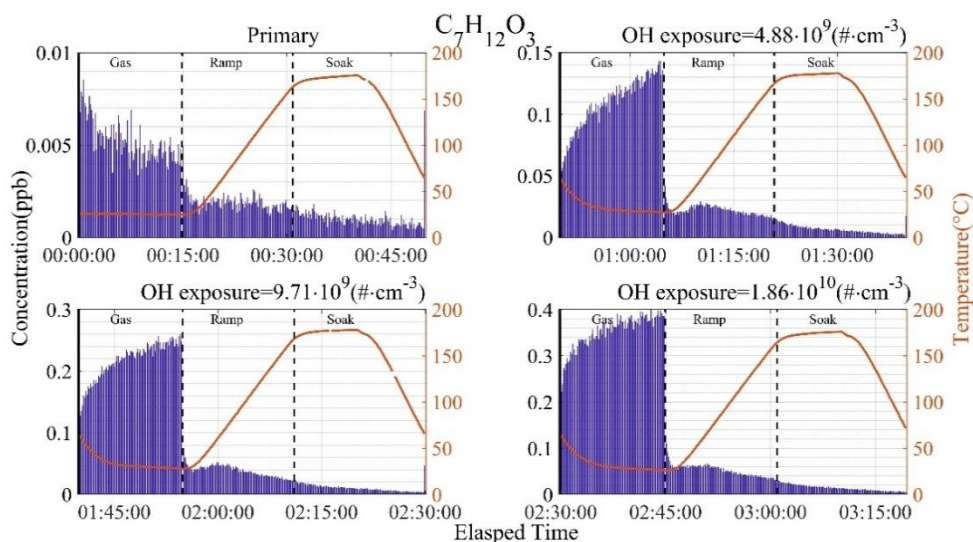
Figure S42 Concentration time series of compound with elemental composition of $C_7H_{12}O_3$ (possibly hydroxy heptanoic acid) at different oxidative stage during FIAGERO measurement of flow tube experiment.
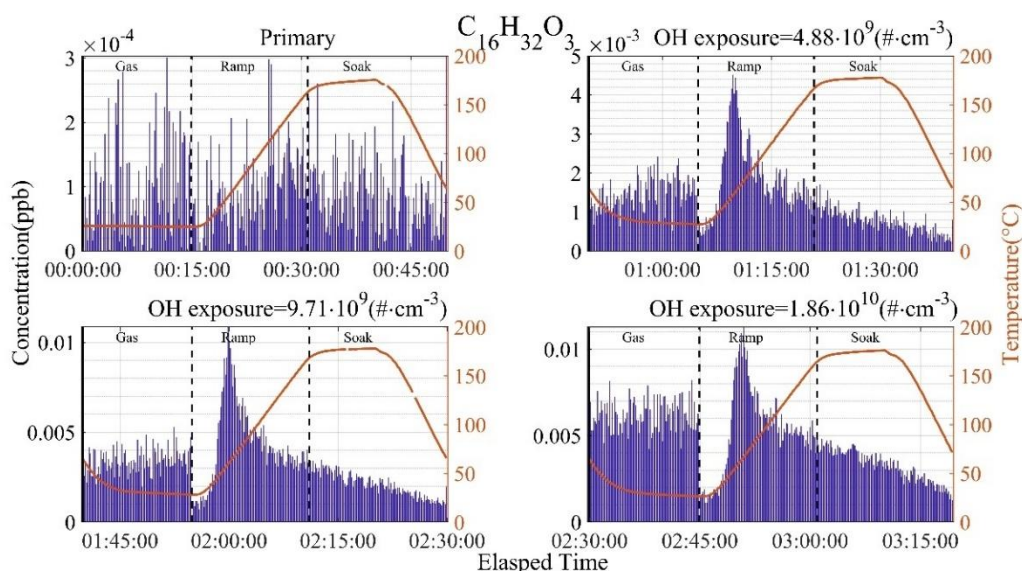
Figure S43 Concentration time series of compound with elemental composition of $C_{16}H_{32}O_3$ (probably hydroxy palmitic acid) at different oxidative stage during FIAGERO measurement of flow tube experiment.
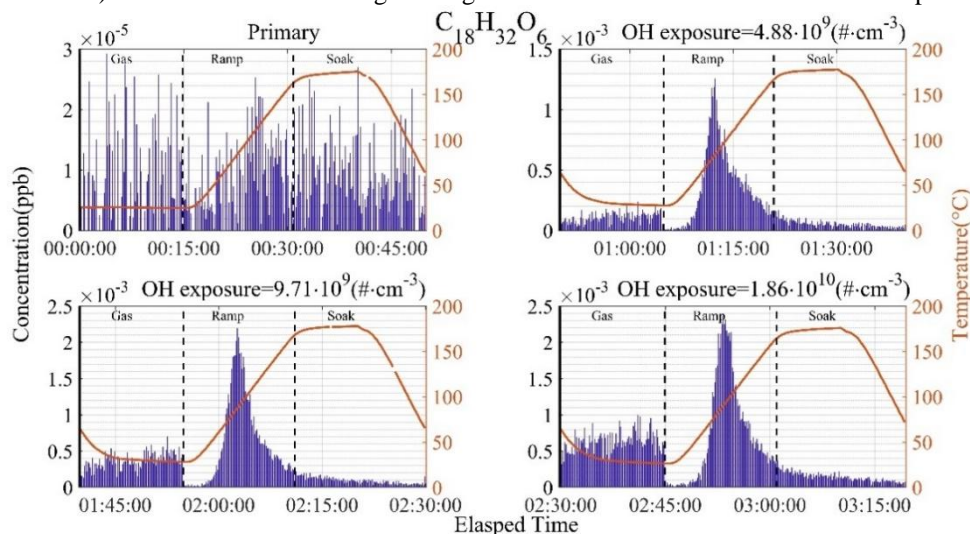
Figure S44 Concentration time series of compound with elemental composition of $C_{18}H_{32}O_6$ at different oxidative stage during FIAGERO measurement of flow tube experiment.
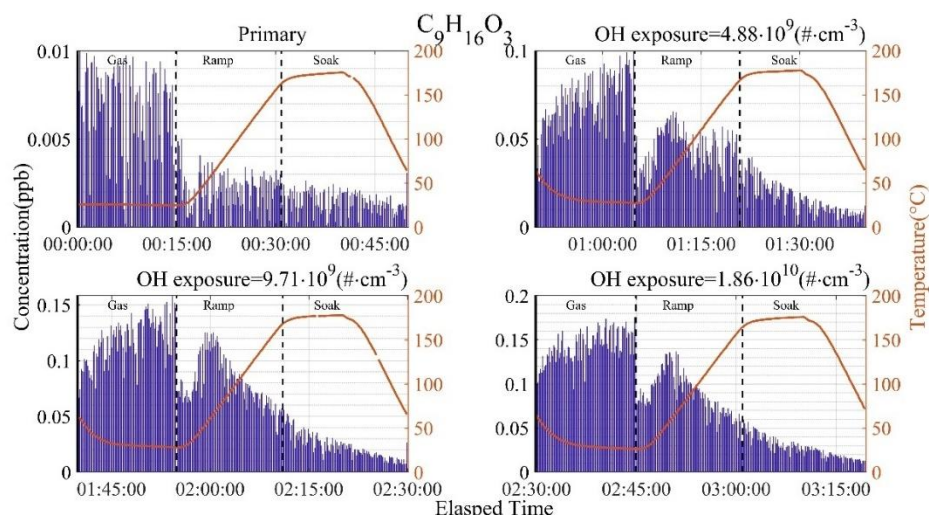
Figure S45 Concentration time series of compound with elemental composition of $C_9H_{16}O_3$ (possibly oxo-nonanoic acids) at different oxidative stage during FIAGERO measurement of flow tube experiment.
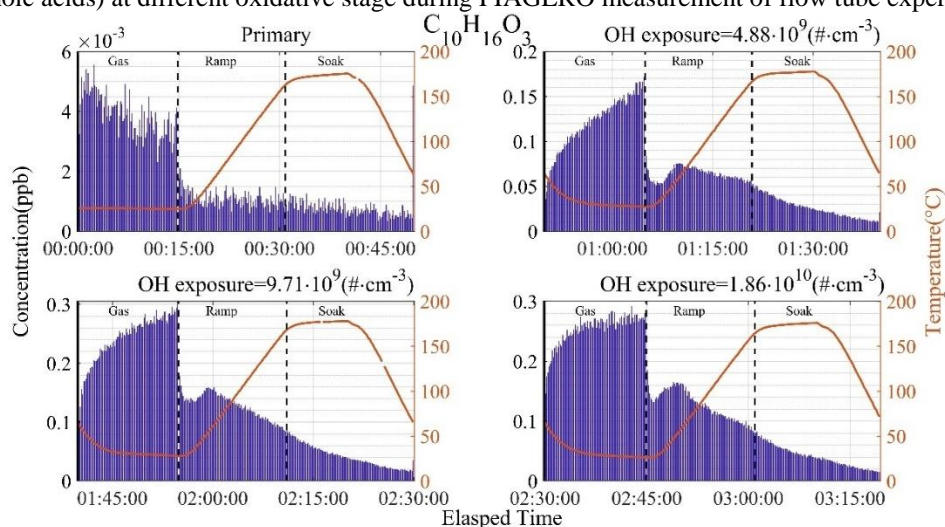
Figure S46 Concentration time series of compound with elemental composition of $C_{10}H_{16}O_3$ (possibly oxo-decenenoic acids) at different oxidative stage during FIAGERO measurement of flow tube experiment.
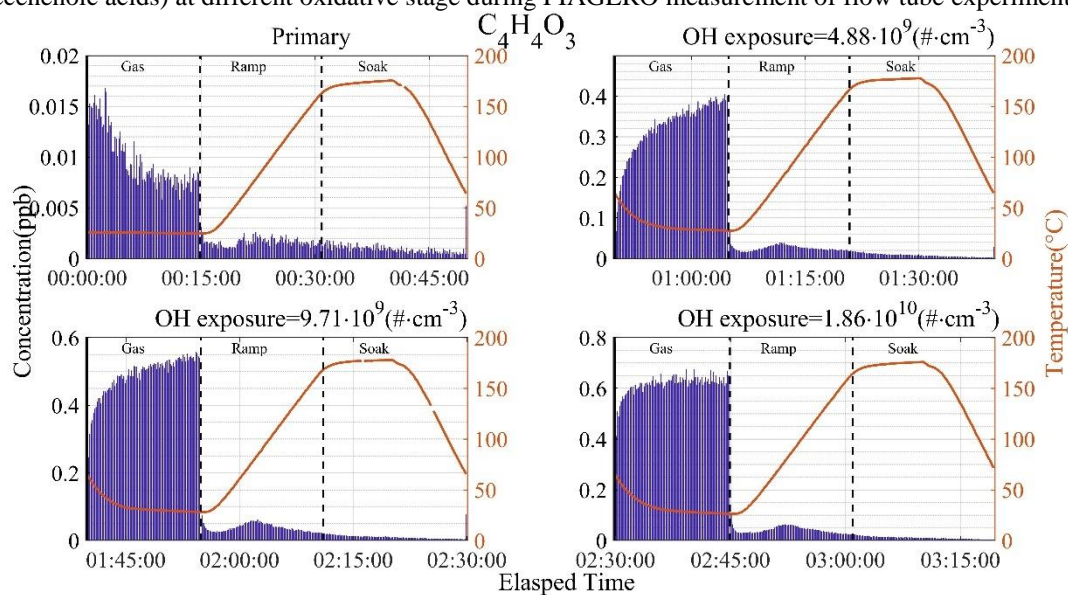
Figure S47 Concentration time series of compound with elemental composition of $C_4H_4O_3$ (possibly oxo-butenoic acids) at different oxidative stage during FIAGERO measurement of flow tube experiment.

Table S13 Average composition and top-20 most abundant species in Factor V4 from ME-2 PMF results

Factor Name: Factor V4

Average elemental composition:
$C_{4.84}H_{8.22}O_{3.88}N_{0.03}S_{0.10}$
MW=131.97 OS$_C$=0.437

Molecular composition:

Molecules	MW(g·mol^{-1})	Relative Intensity	Possible species
$C_2H_4O_4$	92.01	0.72	Hydroperoxyl acetic acid
$C_3H_4O_4$	104.01	0.35	Malonic acid
$C_2H_2O_4$	89.99	0.22	Oxalic acid
$C_7H_{12}O_4$	160.07	0.22	Pimelic acid
$C_7H_{14}O_4$	162.09	0.21	Dihydroxy heptanoic acid
$C_7H_{12}O_5$	176.07	0.18	Hydroxy pimelic acid
$C_6H_{10}O_4$	146.06	0.15	Adipic acid
$C_2H_4O_2$	60.02	0.15	Acetic acid
$C_2H_6S_2$	93.99	0.14	-
$C_3H_6O_4$	106.03	0.13	Glyceric acid
$C_3H_4O_2$	72.02	0.11	Acrylic acid
$C_3H_4O_3$	88.01	0.11	Pyruvic acid
$C_3H_6S_2$	105.99	0.10	-
CH_2O_3	62.00	0.091	-
$C_9H_{16}O_4$	188.10	0.089	Azelaic acid
$C_6H_{12}O_4$	148.07	0.086	Dihydroxy hexanoic Acid
$C_{10}H_{18}O_4$	202.12	0.070	Sebacic acid
$C_6H_{10}O_3$	130.06	0.069	Oxo-hexanoic Acid
$C_7H_{12}O_6$	192.06	0.058	Hydroperoxyl pimelic acid
$C_4H_6O_5$	134.02	0.057	Malic acid

Table S14 Average composition and top-20 most abundant species in Factor V5 from ME-2 PMF results

Factor Name: Factor V5

Average elemental composition:
$C_{6.43}H_{10.62}O_{4.40}N_{0.02}S_{0.06}$
MW=160.40 OS$_C$=-0.035

Molecular composition:

Molecules	MW(g·mol^{-1})	Relative Intensity	Possible species
$C_3H_4O_4$	104.01	0.40	Malonic acid
$C_7H_{12}O_5$	176.07	0.37	Hydroxy pimelic acid
$C_6H_{10}O_4$	146.06	0.32	Adipic acid
$C_6H_{10}O_3$	130.06	0.26	Oxo-hexanoic Acid
$C_6H_{12}O_3$	132.08	0.26	Hydroxy hexanoic acid
$C_2H_4O_2$	60.02	0.22	Acetic acid
$C_7H_{12}O_6$	192.06	0.20	Hydroperoxyl pimelic acid
$C_7H_{14}O_4$	162.09	0.18	Hydroperoxyl heptanoic acid
$C_7H_{12}O_4$	160.07	0.18	Pimelic acid
$C_6H_{12}O_4$	148.07	0.17	Dihydroxy hexanoic Acid
$C_5H_8O_3$	116.05	0.15	Oxo-pentanoic acid
$C_7H_{10}O_6$	190.05	0.15	Hydroxy oxo-pimelic acid
$C_3H_6O_4$	106.03	0.14	Glyceric acid
$C_2H_2O_4$	90.00	0.13	Oxalic acid
$C_4H_6O_4$	118.02	0.12	Succinic acid
$C_2H_4O_4$	92.01	0.11	Hydroperoxyl acetic acid

Molecules	MW	Relative Intensity	Possible species
$C_2H_6S_2$	93.99	0.11	-
$C_8H_{14}O_6$	206.08	0.11	Dihydroxy suberic acid
$C_7H_{14}O_5$	178.08	0.097	Hydroxy hydroperoxy pentanoic acid
$C_{10}H_{16}O_6$	232.09	0.095	Decanetrioic acid

Table S15 Average composition and top-20 most abundant species in Factor SV3 from ME-2 PMF results

Factor Name: Factor SV3			
Average elemental composition: $C_{7.75}H_{13.32}O_{4.49}N_{0.00}S_{0.01}$ MW=178.52 OS$_C$=-0.362			
Molecular composition:			
Molecules	MW(g·mol^{-1})	Relative Intensity	Possible species
$C_3H_4O_4$	104.01	0.47	Malonic acid
$C_9H_{16}O_4$	188.10	0.36	Azelaic acid
$C_{10}H_{18}O_4$	202.12	0.34	Sebacic acid
$C_9H_{18}O_4$	190.12	0.29	Hydroperoxyl nonanoic acid
$C_6H_{12}O_4$	148.07	0.26	Dihydroxy hexanoic acid
$C_7H_{14}O_4$	162.09	0.25	Hydroperoxyl heptanoic acid
$C_9H_{16}O_5$	204.10	0.24	Hydroxy azelaic acid
$C_{10}H_{18}O_5$	218.12	0.21	Hydroxy sebacic acid
$C_7H_{14}O_5$	178.08	0.16	Hydroxy hydroperoxyl pentanoic acid
$C_9H_{18}O_5$	206.12	0.15	Hydroxy hydroperoxyl nonanoic acid
$C_7H_{12}O_5$	176.07	0.13	Hydroxy pimelic acid
$C_6H_{10}O_4$	146.06	0.11	Adipic acid
$C_{10}H_{16}O_6$	232.09	0.10	Decanetrioic acid
$C_7H_{12}O_4$	160.07	0.10	Pimelic acid
$C_9H_{14}O_6$	218.08	0.10	Hydroxy oxo-azelaic acid
$C_9H_{14}O_5$	202.08	0.10	Oxo- azelaic acid
$C_{10}H_{16}O_5$	216.10	0.10	Oxo-sebacic acid
$C_6H_{12}O_5$	164.07	0.091	Hydroxy hydroperoxyl hexanoic acid
$C_4H_6O_5$	134.02	0.083	Malic acid
$C_8H_{16}O_4$	176.10	0.073	Dihydroxy octanoic acid

Table S16 Average composition and top-20 most abundant species in Factor LV2 from ME-2 PMF results

Factor Name: FactorLV2			
Average elemental composition: $C_{6.99}H_{12.16}O_{4.04}N_{0.00}S_{0.00}$ MW=160.77 OSC=-0.317			
Molecular composition:			
Molecules	MW(g·mol^{-1})	Relative Intensity	Possible species
$C_3H_4O_4$	104.01	0.57	Malonic acid
$C_9H_{16}O_4$	188.10	0.40	Azelaic acid
$C_7H_{14}O_4$	162.09	0.35	Hydroperoxyl heptanoic acid
$C_9H_{18}O_4$	190.12	0.29	Hydroperoxyl nonanoic acid
$C_6H_{12}O_4$	148.07	0.28	Dihydroxy hexanoic acid
$C_{10}H_{18}O_4$	202.12	0.23	Sebacic acid
$C_6H_{10}O_4$	146.06	0.19	Adipic acid
$C_7H_{12}O_4$	160.07	0.15	Pimelic acid
$C_3H_4O_3$	88.02	0.14	Pyruvic acid
$C_7H_{12}O_5$	176.07	0.11	Hydroxy pimelic acid
$C_6H_{12}O_3$	132.08	0.11	Hydroxy hexanoic acid

Molecules	MW(g·mol⁻¹)	Relative Intensity	Possible species
$C_9H_{16}O_5$	204.10	0.10	Hydroxy azelaic acid
$C_9H_{14}O_4$	186.09	0.10	Nonendioic acid
$C_{10}H_{16}O_4$	200.10	0.097	Decendioic acid
$C_8H_{16}O_4$	176.10	0.076	Hydroperoxyl octanoic acid
$C_9H_{14}O_5$	202.08	0.067	Oxo-azelaic acid
$C_2H_2O_4$	90.00	0.060	Oxalic acid
$C_{10}H_{16}O_3$	184.11	0.058	Oxo-decanoic acid
$C_{10}H_{18}O_5$	218.11	0.056	Hydroxy sebacic acid
$C_6H_{10}O_3$	130.06	0.049	Oxo-hexanoic Acid

Table S17 Average composition and top-20 most abundant species in Factor LV3 from ME-2 PMF results

Factor Name: FactorLV3

Average elemental composition:
$C_{7.14}H_{11.95}O_{4.11}N_{0.01}S_{0.01}$
MW=163.77 OS$_C$=-0.302

Molecular composition:

Molecules	MW(g·mol⁻¹)	Relative Intensity	Possible species
$C_3H_4O_4$	104.01	0.50	Malonic acid
$C_9H_{16}O_4$	188.10	0.36	Azelaic acid
$C_7H_{14}O_4$	162.09	0.36	Hydroperoxyl heptanoic acid
$C_6H_{10}O_4$	146.06	0.36	Adipic acid
$C_6H_{12}O_3$	132.08	0.34	Hydroxy hexanoic acid
$C_7H_{12}O_4$	160.07	0.25	Pimelic acid
$C_6H_{12}O_4$	148.07	0.18	Dihydroxy hexanoic acid
$C_4H_6O_4$	118.02	0.12	Succinic acid
$C_6H_{10}O_3$	130.06	0.11	Oxo-hexanoic Acid
$C_9H_{14}O_4$	186.09	0.10	Nonendioic acid
$C_3H_6O_4$	106.03	0.10	Glyceric acid
$C_7H_{12}O_5$	176.07	0.10	Hydroxy pimelic acid
$C_{10}H_{16}O_3$	184.11	0.081	Oxo-decanoic acid
$C_{10}H_{16}O_6$	232.09	0.080	Decanetrioic acid
$C_{10}H_{18}O_5$	218.12	0.076	Hydroxy sebacic acid
$C_{10}H_{16}O_4$	200.10	0.075	Decendioic acid
$C_9H_{16}O_5$	204.10	0.070	Hydroxy azelaic acid
$C_4H_4O_3$	100.02	0.070	Oxo-butenoic acid
$C_{10}H_{16}O_5$	216.10	0.064	Oxo-sebacic acid
$C_9H_{14}O_5$	202.08	0.062	Oxo-azelaic acid

Table S18 Average composition and top-20 most abundant species in Factor LV4 from ME-2 PMF results

Factor Name: FactorLV4

Average elemental composition:
$C_{6.47}H_{11.47}O_{4.16}N_{0.00}S_{0.00}$
MW=155.90 OS$_C$=-0.202

Molecular composition:

Molecules	MW(g·mol⁻¹)	Relative Intensity	Possible species
$C_3H_4O_4$	104.01	0.62	Malonic acid
$C_7H_{14}O_4$	162.09	0.49	Hydroperoxyl heptanoic acid
$C_6H_{12}O_4$	148.07	0.45	Dihydroxy hexanoic acid
$C_9H_{16}O_4$	188.10	0.21	Azelaic acid
$C_9H_{18}O_4$	190.12	0.16	Hydroperoxyl nonanoic acid
$C_7H_{12}O_5$	176.07	0.15	Hydroxy pimelic acid

$C_{10}H_{18}O_4$	202.12	0.11	Sebacic acid
$C_7H_{12}O_4$	160.07	0.11	Pimelic acid
$C_6H_{10}O_4$	146.06	0.11	Adipic acid
$C_9H_{16}O_5$	204.10	0.088	Hydroxy azelaic acid
$C_8H_{16}O_4$	176.10	0.085	Hydroperoxyl octanoic acid
$C_9H_{14}O_4$	186.09	0.070	Nonendioic acid
$C_4H_6O_4$	118.02	0.059	Succinic acid
$C_3H_6O_4$	106.03	0.053	Glyceric acid
$C_8H_{14}O_5$	190.08	0.051	Hydroxy suberic acid
$C_{10}H_{16}O_4$	200.10	0.046	Decendioic acid
$C_9H_{14}O_5$	202.08	0.039	Oxo-azelaic acid
$C_2H_2O_4$	90.00	0.038	Oxalic acid
$C_8H_{14}O_4$	174.09	0.035	Suberic acid
$C_4H_4O_4$	116.01	0.032	Fumaric acid
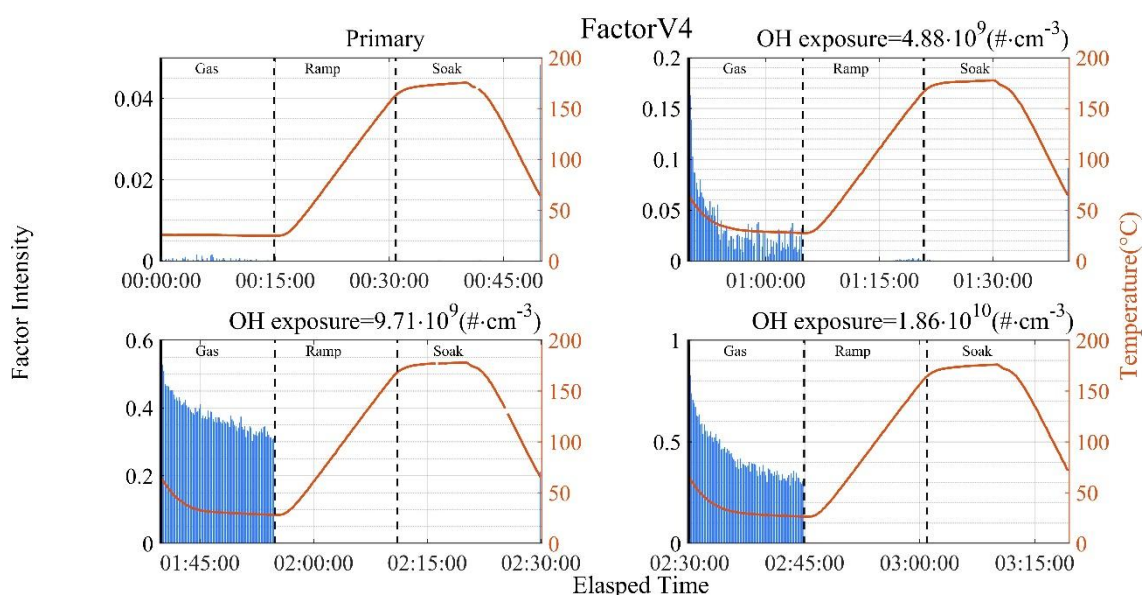
Figure S48 Intensity time series of volatile highly-oxidated product factor V4 (presented remarkably only in gas phase) in PMF results at different oxidative stage during FIAGERO measurement circles.
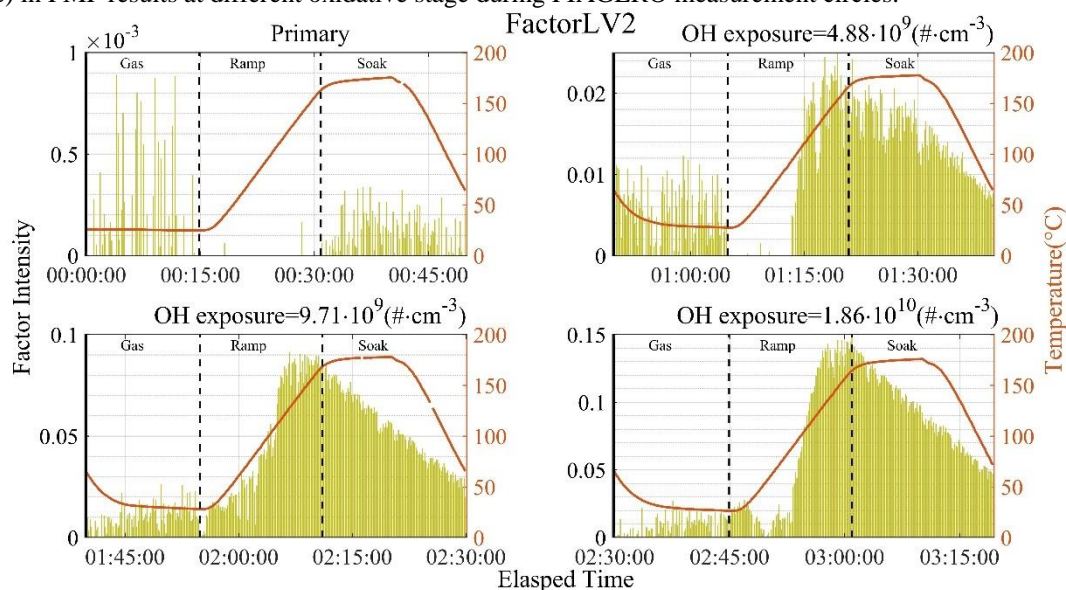
Figure S49 Intensity time series of low-volatile highly-oxidated product factor LV2 (presented remarkably only in aerosol phase) in PMF results at different oxidative stage during FIAGERO measurement circles.
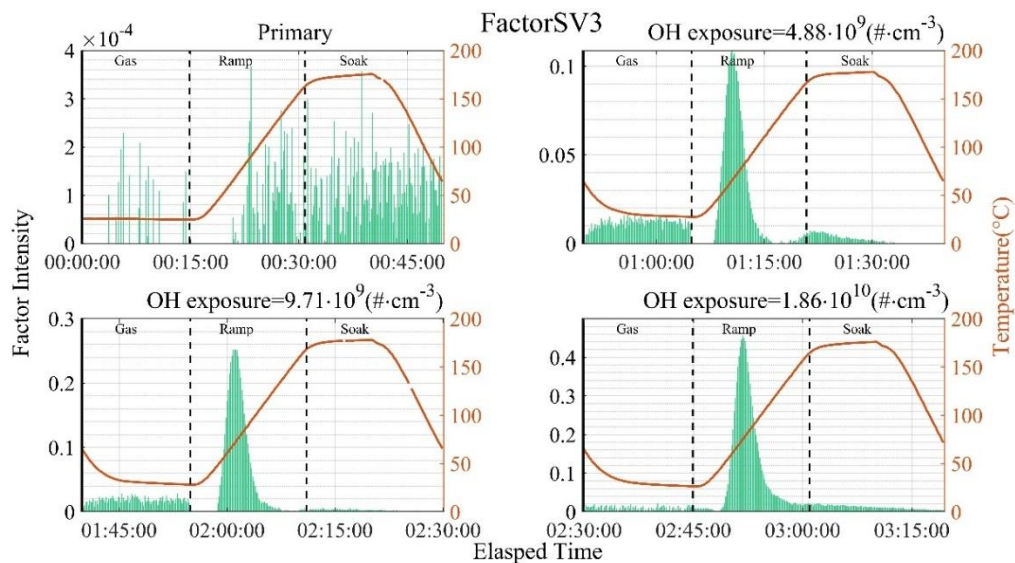
Figure S50 Intensity time series of semi-volatile highly-oxidated product factor SV3 (presented dominantly in aerosol phase) in PMF results at different oxidative stage during FIAGERO measurement circles.
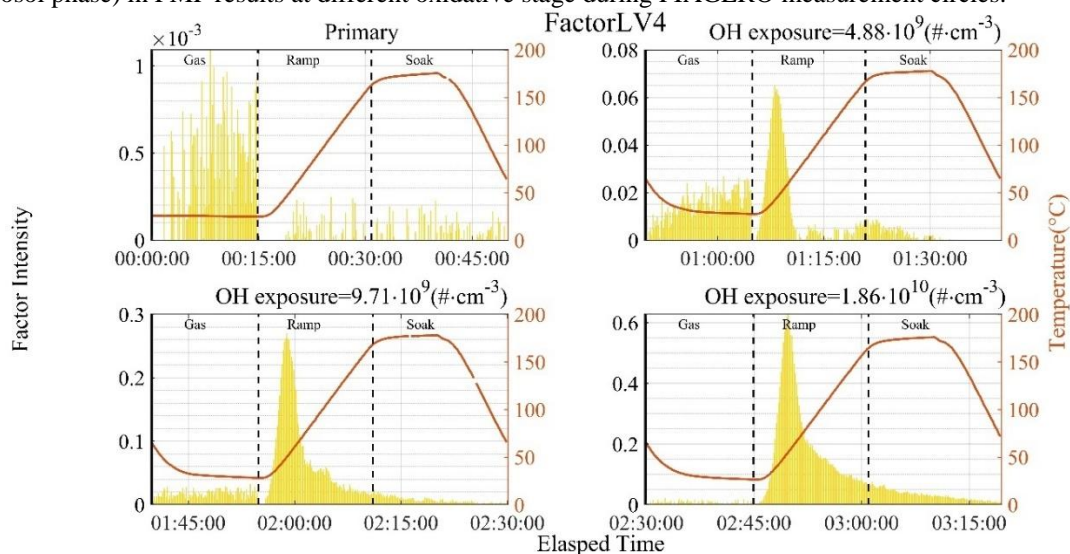
Figure S51 Intensity time series of low-volatile highly-oxidated product factor LV4 (presented remarkably only in aerosol phase) in PMF results at different oxidative stage during FIAGERO measurement circles.
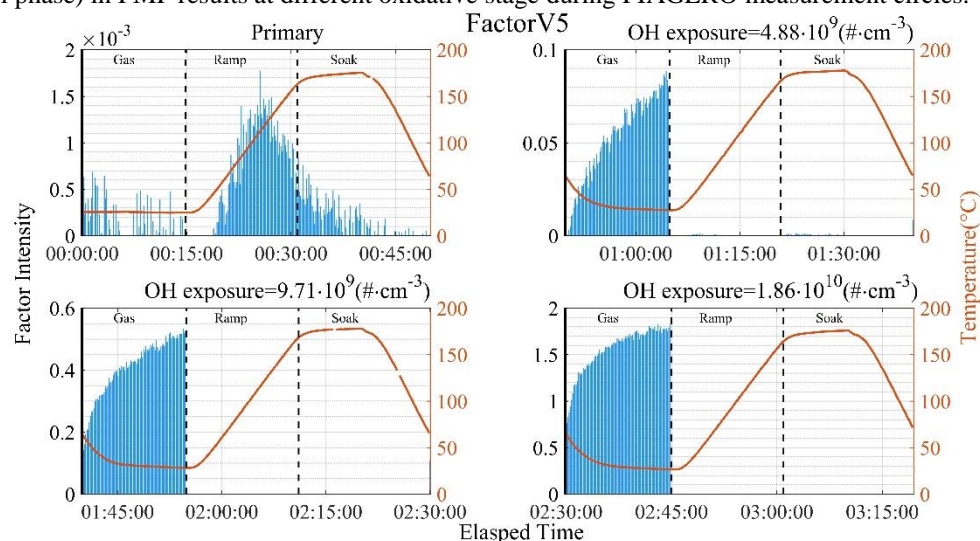
Figure S52 Intensity time series of volatile highly-oxidated product factor V5 (presented remarkably only in gas phase) in PMF results at different oxidative stage during FIAGERO measurement circles.
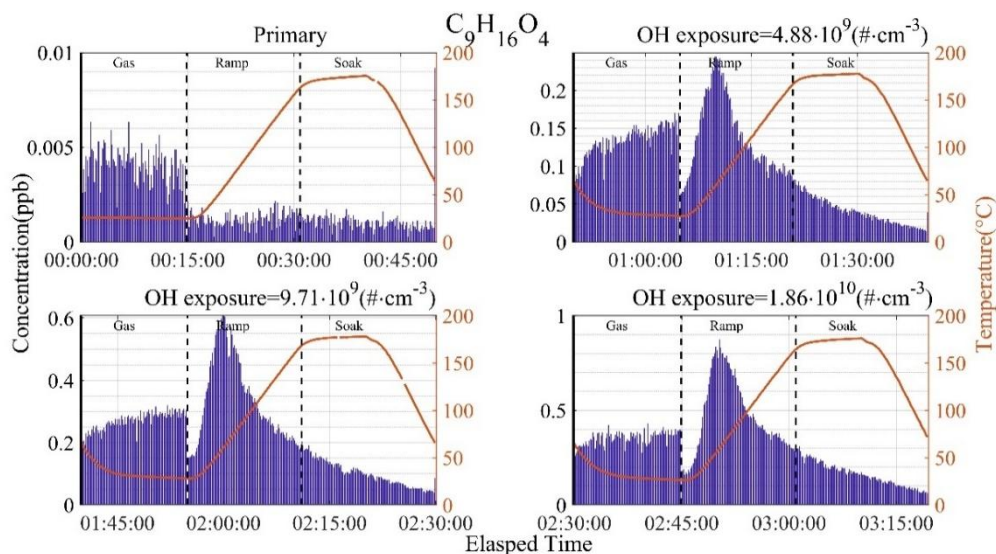
Figure S53 Concentration time series of compound with elemental composition of $C_9H_{16}O_4$ (probably azelaic acid) at different oxidative stage during FIAGERO measurement of flow tube experiment.
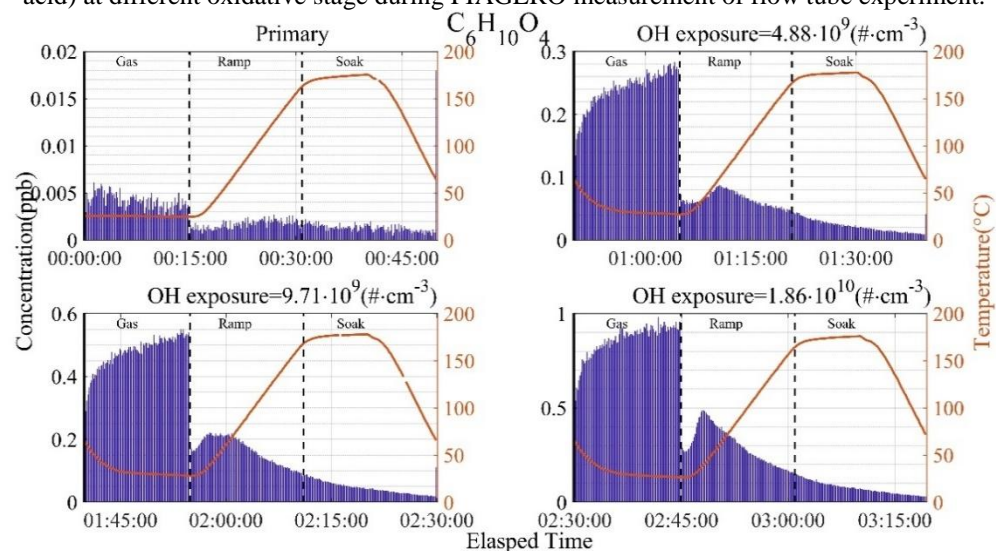
Figure S54 Concentration time series of compound with elemental composition of $C_6H_{10}O_4$ (probably adipic acid) at different oxidative stage during FIAGERO measurement of flow tube experiment.
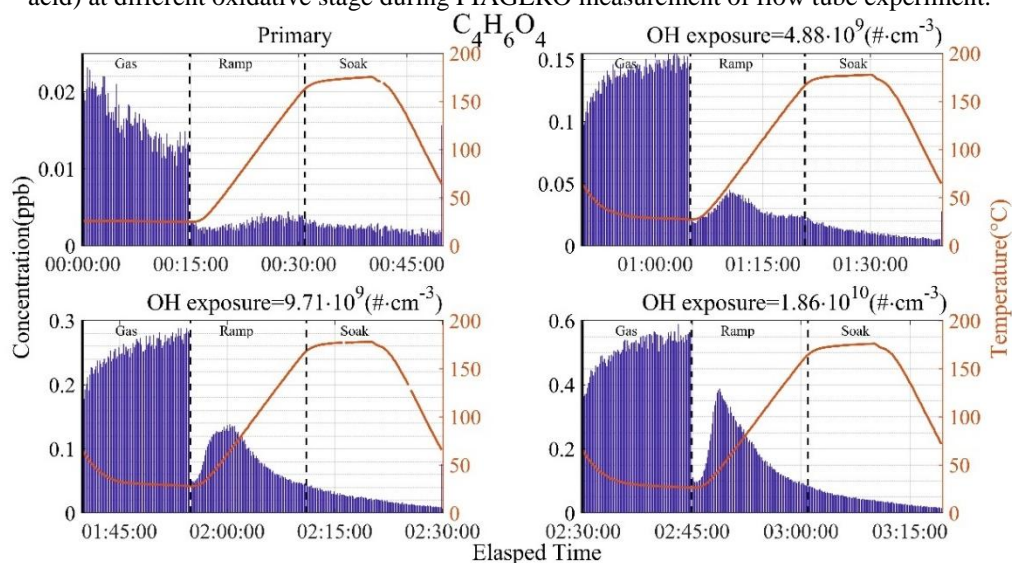
Figure S55 Concentration time series of compound with elemental composition of $C_4H_6O_4$ (probably succinic acid) at different oxidative stage during FIAGERO measurement of flow tube experiment.
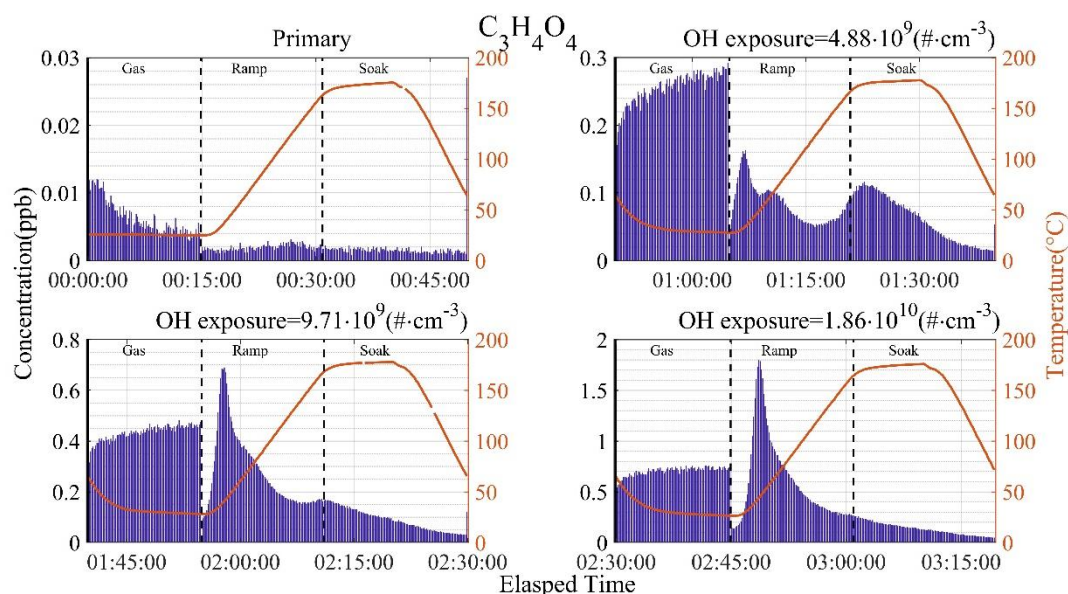
Figure S56 Concentration time series of compound with elemental composition of $C_3H_4O_4$ (probably malonic acid) at different oxidative stage during FIAGERO measurement of flow tube experiment.

Table S19 Average composition and top-20 most abundant species in Factor Unknown from ME-2 PMF results

Factor Name: Unknown			
Average elemental composition:			
$C_{5.93}H_{10.15}O_{3.81}N_{0.00}S_{0.00}$			
MW=142.37 OS$_C$=-0.129			
Molecular composition:			
Molecules	MW(g·mol^{-1})	Relative Intensity	Possible species
$C_3H_4O_4$	104.01	0.68	Malonic acid
$C_6H_{10}O_4$	146.06	0.44	Adipic acid
$C_7H_{12}O_4$	160.07	0.28	Pimelic acid
$C_7H_{14}O_4$	162.09	0.22	Hydroperoxyl heptanoic acid
$C_6H_{12}O_4$	148.07	0.21	Dihydroxy hexanoic acid
$C_9H_{16}O_4$	188.10	0.21	Azelaic acid
$C_6H_{12}O_3$	132.08	0.20	Hydroxy hexanoic acid
$C_6H_{10}O_3$	130.06	0.11	Oxo hexanoic acid
$C_3H_6O_4$	106.03	0.10	Glyceric acid
$C_{10}H_{16}O_3$	184.11	0.10	Oxo-decanoic acid
$C_4H_6O_4$	118.03	0.089	Succinic acid
$C_7H_{12}O_5$	176.07	0.079	Hydroxy pimelic acid
$C_9H_{14}O_4$	186.09	0.076	Nonendioic acid
$C_3H_4O_3$	88.02	0.076	Pyruvic acid
$C_2H_2O_4$	90.00	0.062	Oxalic acid
$C_8H_{14}O_4$	174.09	0.049	Suberic acid
$C_7H_{14}O_3$	146.09	0.048	Hydroxy heptanoic acid
$C_5H_8O_4$	132.04	0.041	Glutaric acid
$C_8H_{16}O_4$	176.10	0.039	Hydroperoxyl octanoic acid
$C_7H_{12}O_3$	144.08	0.039	Hydroxy heptanoic acid

References:

1.   Peng, Z.; Jimenez, J. L., Radical chemistry in oxidation flow reactors for atmospheric chemistry research. *Chem Soc Rev* **2020,** *49* (9), 2570-2616.

2.   Peng, Z.; Day, D. A.; Ortega, A. M.; Palm, B. B.; Hu, W.; Stark, H.; Li, R.; Tsigaridis, K.; Brune, W. H.; Jimenez, J. L., Non-OH chemistry in oxidation flow reactors for the study of atmospheric chemistry systematically examined by modeling. *Atmos. Chem. Phys.* **2016,** *16* (7), 4283-4305.

3.   Sitzmann, M.; Zakharov, A. V.; Pàmies, L. G.; Nicklaus, M. C., NCI/CADD chemical structure Web services. *Abstracts of Papers of the American Chemical Society* **2013,** *245*.

4.   EPA., U. *Estimation Programs Interface Suite™ for Microsoft® Windows, v 4.11*, United States Environmental Protection Agency: Washington, DC, USA., 2012.

5.   Ono, R.; Nakagawa, Y.; Tokumitsu, Y.; Matsumoto, H.; Oda, T., Effect of humidity on the production of ozone and other radicals by low-pressure mercury lamps. *Journal of Photochemistry and Photobiology A: Chemistry* **2014,** *274*, 13-19.

6.   Atkinson, R.; Baulch, D. L.; Cox, R. A.; Crowley, J. N.; Hampson, R. F.; Hynes, R. G.; Jenkin, M. E.; Rossi, M. J.; Troe, J., Evaluated kinetic and photochemical data for atmospheric chemistry: Volume I - gas phase reactions of Ox, HOx, NOx and SOx species. *Atmos. Chem. Phys.* **2004,** *4* (6), 1461-1738.

7.   Yu, Y.; Guo, S.; Wang, H.; Shen, R.; Zhu, W.; Tan, R.; Song, K.; Zhang, Z.; Li, S.; Chen, Y.; Hu, M., Importance of Semivolatile/Intermediate-Volatility Organic Compounds to Secondary Organic Aerosol Formation from Chinese Domestic Cooking Emissions. *Environmental Science & Technology Letters* **2022,** *9* (6), 507-512.

8.   Ylisirniö, A.; Barreira, L. M. F.; Pullinen, I.; Buchholz, A.; Jayne, J.; Krechmer, J. E.; Worsnop, D. R.; Virtanen, A.; Schobesberger, S., On the calibration of FIGAERO-ToF-CIMS: importance and impact of calibrant delivery for the particle-phase calibration. *Atmospheric Measurement Techniques* **2021,** *14* (1), 355-367.

9.   Lopez-Hilfiker, F. D.; Mohr, C.; Ehn, M.; Rubach, F.; Kleist, E.; Wildt, J.; Mentel, T. F.; Lutz, A.; Hallquist, M.; Worsnop, D.; Thornton, J. A., A novel method for online analysis of gas and particle composition: description and evaluation of a Filter Inlet for Gases and AEROsols (FIGAERO). *Atmospheric Measurement Techniques* **2014,** *7* (4), 983-1001.

10.   Stark, H.; Yatavelli, R. L. N.; Thompson, S. L.; Kang, H.; Krechmer, J. E.; Kimmel, J. R.; Palm, B. B.; Hu, W.; Hayes, P. L.; Day, D. A.; Campuzano-Jost, P.; Canagaratna, M. R.; Jayne, J. T.; Worsnop, D. R.; Jimenez, J. L., Impact of Thermal Decomposition on Thermal Desorption Instruments: Advantage of Thermogram Analysis for Quantifying Volatility Distributions of Organic Species. *Environ Sci Technol* **2017,** *51* (15), 8491-8500.

11.   Bannan, T. J.; Le Breton, M.; Priestley, M.; Worrall, S. D.; Bacak, A.; Marsden, N. A.; Mehra, A.; Hammes, J.; Hallquist, M.; Alfarra, M. R.; Krieger, U. K.; Reid, J. P.; Jayne, J.; Robinson, W.; McFiggans, G.; Coe, H.; Percival, C. J.; Topping, D., A method for extracting calibrated volatility information from the FIGAERO-HR-ToF-CIMS and its experimental application. *Atmospheric Measurement Techniques* **2019,** *12* (3), 1429-1439.

12.   Nah, T.; Xu, L.; Osborne-Benthaus, K. A.; White, S. M.; France, S.; Ng, N. L., Mixing order of sulfate aerosols and isoprene epoxydiols affects secondary organic aerosol formation in chamber experiments. *Atmospheric Environment* **2019,** *217*, 116953.

13.   Joo, T.; Rivera-Rios, J. C.; Takeuchi, M.; Alvarado, M. J.; Ng, N. L., Secondary Organic Aerosol Formation from Reaction of 3-Methylfuran with Nitrate Radicals. *ACS Earth and Space Chemistry* **2019,** *3* (6), 922-934.

14.   Ye, Q.; Wang, M.; Hofbauer, V.; Stolzenburg, D.; Chen, D.; Schervish, M.; Vogel, A.; Mauldin, R. L.; Baalbaki, R.; Brilke, S.; Dada, L.; Dias, A.; Duplissy, J.; El Haddad, I.; Finkenzeller, H.; Fischer, L.; He, X.; Kim, C.; Kürten, A.; Lamkaddam, H.; Lee, C. P.; Lehtipalo, K.; Leiminger, M.; Manninen, H. E.; Marten, R.; Mentler, B.; Partoll, E.; Petäjä, T.; Rissanen, M.; Schobesberger, S.; Schuchmann, S.; Simon, M.; Tham, Y. J.; Vazquez-Pufleau, M.; Wagner, A. C.; Wang, Y.; Wu, Y.; Xiao, M.; Baltensperger, U.; Curtius, J.; Flagan, R.; Kirkby, J.; Kulmala, M.; Volkamer, R.; Winkler, P. M.; Worsnop, D.; Donahue, N. M., Molecular Composition and Volatility of Nucleated Particles from α-Pinene Oxidation between −50 °C and +25 °C. *Environmental Science & Technology* **2019,** *53* (21), 12357-12365.

15.   Wang, M.; Chen, D.; Xiao, M.; Ye, Q.; Stolzenburg, D.; Hofbauer, V.; Ye, P.; Vogel, A.

L.; Mauldin, R. L., 3rd; Amorim, A.; Baccarini, A.; Baumgartner, B.; Brilke, S.; Dada, L.; Dias, A.; Duplissy, J.; Finkenzeller, H.; Garmash, O.; He, X. C.; Hoyle, C. R.; Kim, C.; Kvashnin, A.; Lehtipalo, K.; Fischer, L.; Molteni, U.; Petaja, T.; Pospisilova, V.; Quelever, L. L. J.; Rissanen, M.; Simon, M.; Tauber, C.; Tome, A.; Wagner, A. C.; Weitz, L.; Volkamer, R.; Winkler, P. M.; Kirkby, J.; Worsnop, D. R.; Kulmala, M.; Baltensperger, U.; Dommen, J.; El-Haddad, I.; Donahue, N. M., Photo-oxidation of Aromatic Hydrocarbons Produces Low-Volatility Organic Compounds. *Environ Sci Technol* **2020,** *54* (13), 7911-7921.

16.   Donahue, N. M.; Epstein, S. A.; Pandis, S. N.; Robinson, A. L., A two-dimensional volatility basis set: 1. organic-aerosol mixing thermodynamics. *Atmospheric Chemistry and Physics* **2011,** *11* (7), 3303-3318.

17.   Li, Y.; Pöschl, U.; Shiraiwa, M., Molecular corridors and parameterizations of volatility in the chemical evolution of organic aerosols. *Atmospheric Chemistry and Physics* **2016,** *16* (5), 3327-3344.

18.   Schymanski, E. L.; Jeon, J.; Gulde, R.; Fenner, K.; Ruff, M.; Singer, H. P.; Hollender, J., Identifying small molecules via high resolution mass spectrometry: Communicating confidence. *Environ. Sci. Technol.* **2014,** *48* (4), 2097-2098.

19.   Paatero, P., The Multilinear Engine: A Table-Driven, Least Squares Program for Solving Multilinear Problems, including the n-Way Parallel Factor Analysis Model. *Journal of Computational and Graphical Statistics* **1999,** *8* (4), 854-888.

20.   Canonaco, F.; Crippa, M.; Slowik, J. G.; Baltensperger, U.; Prévôt, A. S. H., SoFi, an IGOR-based interface for the efficient use of the generalized multilinear engine (ME-2) for the source apportionment: ME-2 application to aerosol mass spectrometer data. *Atmospheric Measurement Techniques* **2013,** *6* (12), 3649-3661.

21.   Berry, M. W.; Browne, M.; Langville, A. N.; Pauca, V. P.; Plemmons, R. J., Algorithms and applications for approximate nonnegative matrix factorization. *Computational Statistics & Data Analysis* **2007,** *52* (1), 155-173.

22.   Buchholz, A.; Ylisirniö, A.; Huang, W.; Mohr, C.; Canagaratna, M.; Worsnop, D. R.; Schobesberger, S.; Virtanen, A., Deconvolution of FIGAERO–CIMS thermal desorption profiles using positive matrix factorisation to identify chemical and physical processes during particle evaporation. *Atmos. Chem. Phys.* **2020,** *20* (13), 7693-7716.

23.   Pun, B. K.; Griffin, R. J.; Seigneur, C.; Seinfeld, J. H., Secondary organic aerosol 2. Thermodynamic model for gas/particle partitioning of molecular constituents. *Journal of Geophysical Research: Atmospheres* **2002,** *107* (D17), AAC 4-1-AAC 4-15.

24.   Bougiatioti, A.; Stavroulas, I.; Kostenidou, E.; Zarmpas, P.; Theodosi, C.; Kouvarakis, G.; Canonaco, F.; Prévôt, A. S. H.; Nenes, A.; Pandis, S. N.; Mihalopoulos, N., Processing of biomass-burning aerosol in the eastern Mediterranean during summertime. *Atmospheric Chemistry and Physics* **2014,** *14* (9), 4793-4807.

25.   Pankow, J. F., An absorption model of gas/particle partitioning of organic compounds in the atmosphere. *Atmospheric Environment* **1994,** *28* (2), 185-188.

26.   Odum, J. R.; Yu, J.; Kamens, R. M., Modeling the Mass Transfer of Semivolatile Organics in Combustion Aerosols. *Environmental Science & Technology* **1994,** *28* (13), 2278-2285.

27.   Odum, J. R.; Hoffmann, T.; Bowman, F.; Collins, D.; Flagan, R. C.; Seinfeld, J. H., Gas/Particle Partitioning and Secondary Organic Aerosol Yields. *Environmental Science & Technology* **1996,** *30* (8), 2580-2585.

28.   Pankow, J. F.; Asher, W. E., SIMPOL.1: a simple group contribution method for predicting vapor pressures and enthalpies of vaporization of multifunctional organic compounds. *Atmos. Chem. Phys.* **2008,** *8* (10), 2773-2796.

29.   Compernolle, S.; Ceulemans, K.; Müller, J. F., EVAPORATION: a new vapour pressure estimation methodfor organic molecules including non-additivity and intramolecular interactions. *Atmospheric Chemistry and Physics* **2011,** *11* (18), 9431-9450.

30.   Ren, S.; Yao, L.; Wang, Y.; Yang, G.; Liu, Y.; Li, Y.; Lu, Y.; Wang, L.; Wang, L., Volatility parameterization of ambient organic aerosols at a rural site of the North China Plain. *Atmos. Chem. Phys.* **2022,** *22* (14), 9283-9297.

31.   Chen, W.; Hu, W.; Tao, Z.; Cai, Y.; Cai, M.; Zhu, M.; Ye, Y.; Zhou, H.; Jiang, H.; Li, J.; Song, W.; Zhou, J.; Huang, S.; Yuan, B.; Shao, M.; Feng, Q.; Li, Y.; Isaacman-VanWertz, G.; Stark, H.; Day, D. A.; Campuzano-Jost, P.; Jimenez, J. L.; Wang, X., Quantitative

Characterization of the Volatility Distribution of Organic Aerosols in a Polluted Urban Area: Intercomparison Between Thermodenuder and Molecular Measurements. *Journal of Geophysical Research: Atmospheres* **2024,** *129* (4).

32.   Caudillo, L.; Surdu, M.; Lopez, B.; Wang, M.; Thoma, M.; Bräkling, S.; Buchholz, A.; Simon, M.; Wagner, A. C.; Müller, T.; Granzin, M.; Heinritzi, M.; Amorim, A.; Bell, D. M.; Brasseur, Z.; Dada, L.; Duplissy, J.; Finkenzeller, H.; He, X.-C.; Lamkaddam, H.; Mahfouz, N. G. A.; Makhmutov, V.; Manninen, H. E.; Marie, G.; Marten, R.; Mauldin, R. L.; Mentler, B.; Onnela, A.; Petäjä, T.; Pfeifer, J.; Philippov, M.; Piedehierro, A. A.; Rörup, B.; Scholz, W.; Shen, J.; Stolzenburg, D.; Tauber, C.; Tian, P.; Tomé, A.; Umo, N. S.; Wang, D. S.; Wang, Y.; Weber, S. K.; Welti, A.; Zauner-Wieczorek, M.; Baltensperger, U.; Flagan, R. C.; Hansel, A.; Kirkby, J.; Kulmala, M.; Lehtipalo, K.; Worsnop, D. R.; Haddad, I. E.; Donahue, N. M.; Vogel, A. L.; Kürten, A.; Curtius, J., An intercomparison study of four different techniques for measuring the chemical composition of nanoparticles. *Atmospheric Chemistry and Physics* **2023,** *23* (11), 6613-6631.

33.   Tang, M. J.; Shiraiwa, M.; Pöschl, U.; Cox, R. A.; Kalberer, M., Compilation and evaluation of gas phase diffusion coefficients of reactive trace gases in the atmosphere: Volume 2. Diffusivities of organic compounds, pressure-normalised mean free paths, and average Knudsen numbers for gas uptake calculations. *Atmospheric Chemistry and Physics* **2015,** *15* (10), 5585-5598.

34.   Shiraiwa, M.; Ammann, M.; Koop, T.; Pöschl, U., Gas uptake and chemical aging of semisolid organic aerosol particles. *Proceedings of the National Academy of Sciences* **2011,** *108* (27), 11003.

35.   Miyamoto, S.; Shimono, K., Molecular Modeling to Estimate the Diffusion Coefficients of Drugs and Other Small Molecules. *Molecules* **2020,** *25* (22).

36.   Zwanzig, R.; Harrison, A. K., Modifications of the Stokes–Einstein formula. *The Journal of Chemical Physics* **1985,** *83* (11), 5861-5862.

37.   Li, Y.; Day, D. A.; Stark, H.; Jimenez, J. L.; Shiraiwa, M., Predictions of the glass transition temperature and viscosity of organic aerosols from volatility distributions. *Atmos. Chem. Phys.* **2020,** *20* (13), 8103-8122.

38.   Shiraiwa, M.; Pöschl, U., Mass accommodation and gas–particle partitioning in secondary organic aerosols: dependence on diffusivity, volatility, particle-phase reactions, and penetration depth. *Atmospheric Chemistry and Physics* **2021,** *21* (3), 1565-1580.